

Investigation of the benefits of hydrofoils on sailing vessel performance and adaption of current velocity prediction models

Auteur : Yerkes Medina, Robert Francisco

Promoteur(s) : Rigo, Philippe

Faculté : Faculté des Sciences appliquées

Diplôme : Master : ingénieur civil mécanicien, à finalité spécialisée en "Advanced Ship Design"

Année académique : 2022-2023

URI/URL : <http://hdl.handle.net/2268.2/18234>

Avertissement à l'attention des usagers :

Tous les documents placés en accès ouvert sur le site le site MatheO sont protégés par le droit d'auteur. Conformément aux principes énoncés par la "Budapest Open Access Initiative"(BOAI, 2002), l'utilisateur du site peut lire, télécharger, copier, transmettre, imprimer, chercher ou faire un lien vers le texte intégral de ces documents, les disséquer pour les indexer, s'en servir de données pour un logiciel, ou s'en servir à toute autre fin légale (ou prévue par la réglementation relative au droit d'auteur). Toute utilisation du document à des fins commerciales est strictement interdite.

Par ailleurs, l'utilisateur s'engage à respecter les droits moraux de l'auteur, principalement le droit à l'intégrité de l'oeuvre et le droit de paternité et ce dans toute utilisation que l'utilisateur entreprend. Ainsi, à titre d'exemple, lorsqu'il reproduira un document par extrait ou dans son intégralité, l'utilisateur citera de manière complète les sources telles que mentionnées ci-dessus. Toute utilisation non explicitement autorisée ci-avant (telle que par exemple, la modification du document ou son résumé) nécessite l'autorisation préalable et expresse des auteurs ou de leurs ayants droit.



Master Thesis

Master Sciences, Technologie, Santé

Mention Technologie Marine/Marine Technology

Parcours Hydrodynamics for Ocean Engineering

Investigation of the Benefits of Hydrofoils on Sailing Vessel Performance and Adaption of Current Velocity Prediction Models

Submitted on: 18 August 2023

by

Robert YERKES MEDINA

Supervisor: Prof. Giles BARKLEY



Contents

Declaration of Authorship	iv
Acknowledgements	v
Abstract	vi
List of Figures	vii
List of Tables	viii
List of Symbols	ix
1 INTRODUCTION	1
2 GENERAL THEORY OF SAILING	4
2.1 Wind Vectors	4
2.2 Sail Forces	7
3 VPP GOVERNING EQUATIONS	10
3.1 Resistance and Powering	10
3.1.1 Resistance	10
3.1.2 Powering (Sail Drive Force)	15
3.2 Side Forces	16
3.2.1 Sail Side Force	16
3.2.2 Keel Side Force	17
3.3 Righting and Heeling Moments	18
3.3.1 Righting Moment	18
3.3.2 Heeling Moment	20
4 THREE DEGREE OF FREEDOM VPP	22
4.1 Optimization Problem	22
4.2 Implementation	23
4.3 Validation	25
4.3.1 Direct Experimental Method	26
4.3.2 Inputs	29

4.3.3	Comparison	32
5	ADDITION OF FOILS	38
5.1	Theory of Foiling	38
5.2	Experimental Investigation to Determine Foil Aspect Ratio	44
6	EFFECT OF FOILS ON SAILING PERFORMANCE	48
6.1	Farr 52'	48
6.2	IMOCA Open 60	50
7	CONCLUSION	52
8	APPENDIX	56
8.1	Environmental Parameters	56
8.2	Farr 52' Principle Characteristics	57
8.2.1	Hull Parameters	57
8.2.2	Keel Parameters	57
8.2.3	Bulb Parameters	58
8.2.4	Sail Parameters	58
8.3	Lazare Open 60 Principle Characteristics	59
8.4	Sail Calculations	61
8.4.1	Sail Areas	61
8.4.2	Centers of Effort	61
8.5	Delft Systematic Yacht Hull Series Coefficients	61
8.5.1	Upright Residuary Resistance	63
8.5.2	Heeled Wetted Surface Area	64
8.5.3	Heeled Residuary Resistance	66
8.5.4	Effective Draft of Keel	67
8.5.5	Keel Side Force	68
8.6	Foil Calculations	68
8.6.1	Calculating Apparent Flow Velocity and Angle of Attack	69
8.6.2	Calculating Lift and Drag Forces	71
8.7	Excel Lambda Functions	73
8.7.1	Array of Integer Divisors	74

8.7.2	True Wind Arrays	74
8.7.3	Linear Interpolation	75
8.7.4	Bilinear Interpolation	75
8.8	Excel Macro	76
	REFERENCES	80

Declaration of Authorship

I declare that this thesis and the work presented in it are my own and have been generated by me as the result of my own original research.

Where I have consulted the published work of others, this is always clearly attributed.

Where I have quoted from the work of others, the source is always given. With the exception of such quotations, this thesis is entirely my own work.


I have acknowledged all main sources of help.

Where the thesis is based on work done by myself jointly with others, I have made clear exactly what was done by others and what I have contributed myself.

This thesis contains no material that has been submitted previously, in whole or in part, for the award of any other academic degree or diploma.

I cede copyright of this thesis in favor of École Centrale de Nantes.

Date: 18 August, 2023

Signature: 

Acknowledgements

The author would like to thank all the Faculty of Solent University who not only directly assisted in conducting research but also those who indirectly supported through the administrative processes of enrolment.

In particular, gratitude must be given to Professor Giles Barkley for his passionate guidance and oversight of this project, both of which were instrumental in its successful completion, as well as Professor Vittorio Boccolini for his guidance and motivation and Steve Crook for his assistance in tow tank testing.

Finally, a special thank you to Lazare Gournay who laid the foundation for this work through his master's thesis and the development of the Lazare Open 60 sailing yacht.

Abstract

This paper seeks to develop a Microsoft Excel based Velocity Prediction Program (VPP) capable of estimating performance of sailboats outfitted with hydrofoils. To do so, the general theory underlying the mechanics of sailing is briefly explained before a more in depth discussion of the Delft Systematic Yacht Hull Series (DSYHS) and its accompany regression lines that have been developed over the past several decades. Building off the sailing fundamentals and DSYHS regression lines forces are balanced to create an optimization solver that lies at the heart of the VPP.

The developed three degree of freedom VPP is compared to existing commercial VPP software which is augmented by tow tank testing conducted at Solent University's Hydrodynamics Centre. With suitable agreement, hydrofoils are introduced to the system. After an overview of their history and the theory behind foiling, the mathematics underpinning their utilization is explored. Using lifting line theory to model the effect of foils, their contributions to sailboat performance is addended to the previous solver to develop a four degree of freedom VPP. Finally, the completed VPP is tested and the effects of foils on two different hullforms are explored.

List of Figures

2	Wind speed and angles as experienced by a heeled sailboat	4
3	Wetted surface area versus heel angle for a Farr 52'	6
4	IMS sail lift and drag coefficients	8
5	Wetted surface area comparison	14
6	Plan view of keel and sail forces	16
7	Definition of residuary stability	19
8	VPP Dashboard	25
9	Relationship between resistance and side force (from leeway experiments) .	27
10	Upright resistance curve from experimental data	29
11	Resistance versus side force squared	30
12	Resistance versus side force squared by Froude number	31
13	Side force versus leeway angle	33
14	WinDesign VPP polar diagram	34
15	WinDesign VPP Cartesian diagram	34
16	Comparison of boat speeds between two VPPs	35
17	VPP Cartesian diagram with WinDesign <i>Reef</i> and <i>Flat</i> values	36
18	WinDesign VPP calculated heel angles	36
19	Comparison of the effect of <i>Reef</i> and <i>Flat</i> values on heel angles	37
20	Farr 52' model hydrostatic curves of form	43
21	Lift generated perpendicular to daggerboard	46
22	47
23	Comparison of boat speeds with and without foils	48
24	Reduction in heel angle due to foil	49
25	Comparison of Lazare Open 60 boat speeds with and without foils	50
26	Comparison of change in boat speeds due to AR	51
27	Definition of sail set parameters	59
28	Calculation of apparent flow speed - plan view	69
29	Calculation of apparent flow speed	70
30	Calculation of apparent leeway angle	71
31	Lift and drag forces	72
32	Lift and side forces	72

List of Tables

1	Farr 52' hull parameter summary	27
2	Environmental parameters	56
3	Farr 52' hull parameters	57
4	Keel parameters	58
5	Bulb parameters	58
6	Sail set parameters	59
7	Lazare Open 60 principle characteristics	60
8	Deflt Systematic Yacht Hull Series parameters	63
9	Canoe body upright residuary resistance coefficients	64
10	Keel upright residuary resistance coefficients	65
11	Heeled wetted surface area coefficients	66
12	Canoe body heeled residuary resistance coefficients	67
13	Keel heeled residuary resistance coefficients	67
14	Effective draft coefficients	68
15	Keel side force coefficients	68

List of Symbols

α	Foil static angle of heel	$C_{L,3D}$	3D coefficient of lift
β	Leeway angle	CLR	Center of lateral resistance of hull
β_A	Apparent wind angle	CoE	Center of effort of sails
β_T	True wind angle	CoE_y	Foil horizontal center of effort
Δ	Displacement	CoE_z	Foil vertical center of effort
η	Apparent foil leeway modification	D	Drag
μ	Dynamic viscosity of water	F_D	Drive force
ν	Kinematic viscosity of water	F_H	Heeling force
ϕ	Heel angle	g	Gravitational Acceleration
ρ	Density of water	GM	Metacentric height
ρ_a	Density of air	GZ	Righting lever arm
ε	Residual value	HM	Heeling moment
ξ	Foil apparent angle of attack	I	Second moment of area
A_{Plan}	Foil planform area	k	Form factor
A_W	Waterplane Area	KG	Height of center of gravity
AL_0	Lift area at 0 leeway	KSF	Keel side force
AL_s	Lift curve slope with respect to yaw	L	Lift
AR_e	Effective aspect ratio	L_{WL}	Length along the waterline
B_{WL}	Beam at waterline	LCB	Longitudinal center of buoyancy
BAD	Height of boom above deck	LCF	Longitudinal center of flotation
Bl	Blanketing Factor	MN	Residual stability lever
BM	Metacentric radius	q	Dynamic pressure
C_b	Block Coefficient	R_e	Reynolds' number
C_D	Coefficient of drag	R_r	Residuary Resistance
C_L	Coefficient of lift	$R_{D,3D}$	Drag Resistance of foil
C_p	Prismatic coefficient	RM	Righting moment
C_r	Coefficient of residuary resistance	S_c	Canoe body wetted surface area
$C_{D,2D}$	2D coefficient of drag	$S_{c,\phi}$	Heeled canoe body wetted surface area
$C_{D,3D}$	3D coefficient of drag		
$C_{D,I}$	Coefficient of induced drag	SA	Sail Area
$C_{L,2D}$	2D coefficient of lift	SA_{Ref}	Reference Sail Area

SF	Side force	V_T	True wind speed
SSF	Sail side force	V_f	Apparent foil velocity
T	Draft	Z_e	Vertical center of effort
T_c	Canoe body draft	Z_{cbk}	Vertical center of buoyancy of keel
T_e	Effective draft	∇	Displaced volume
V_A	Apparent wind speed	∇_c	Canoe body displaced volume
V_b	Boat speed	∇_k	Keel displaced volume

1 INTRODUCTION

Solent University in Southampton is well known for its Yacht Design and Production courses which, over the course of three years, teach undergraduate students the fundamentals of naval architecture, yacht design, and material science in order to prepare graduates who are sufficiently capable to enter the maritime design and production industries. As a capstone project of sorts, undergraduate students spend their final year on a cross-disciplinary dissertation where they design a boat from conception up to the production phase taking into consideration, hydrostatics and stability, resistance and propulsion, structural loads in accordance with IMO regulations, as well as general arrangements and aesthetics. For many of the students this is an excellent opportunity to delve deeper into a field naval architecture that they're interested in and create a polished product to help launch their careers in the maritime industry. As many of the students have strong sailing backgrounds (with several even competing at the interational level) it is not uncommon for students to chose to design a sailing yacht for their dissertation, a type of watercraft that Solent University is uniquely suited to supporting with its knowledgeable faculty, numerous industry contacts in the fields, and history of sailing excellence.

To meet evolving needs, the design of sailboats has continually progressed and as the understanding of sailing mechanics has improved, designers have developed yachts outfitted with more efficient, high aspect keels and rudders. Advances in material science and production technologies have further enabled designs that would not have been possible decades prior. Thus, in order for a racing yacht to be competitive it must push both class rules and the capabilities of modern technology. Over the past few decades this has meant the adoption of hydrofoils which increase a vessel's righting moment and lift its hull out of the water, decreasing resistance and enabling the boat to sail considerably faster. Just as the professional sailboat designers who have eagerly adopted foil in the sailing world so to do many of the undergraduate students at Solent University outfit their dissertation sailing vessels with hydrofoils, seeking to learn more about this emerging field while designing a contemporary and relevant boat. Unfortunately, there is not much software available which takes into account the effects of hydrofoils and even less that is digestible at the undergraduate level.

When designing a sailboat, engineers rely not only on parametric analyses of other boats and past experiences but also lean heavily on computational tools such as velocity prediction programs (known as VPPs). As their name suggests, these programs seek to predict the performance of a sailboat, namely its velocity, across a range of wind conditions that a given boat is expected to experience. With the exponential growth of computational abilities the development of VPPs has also grown considerably. However, as with many emerging phenomena, the computational modeling of foils in VPPs lags behind the development and utilization of foils themselves with few, if any, commercially available VPPs being able to implement foils in sailboat designs. WinDesign VPP is provided to the students at Solent University for analysis of sailboat performance, and though it is a powerful computational tool, it does not allow for the direct implementation of foils.

In previous years, this issue was circumvented by overwriting the default GZ curve with one that takes into account any additional righting moment provided by an underwater foil. This simple solution is easily implemented though it suffers from not being able to take into account the hull lifting out of the water. Further, the additional righting moment generated by a foil is itself dependent on speed and leeway of the boat, hence the modified GZ curve is also a function of the wind conditions. This paper, then, seeks to develop a VPP which explicitly takes into account the forces and moments generated by hydrofoils.

This proposed VPP has been developed through the use of Microsoft Excel, which, perhaps baffling to a conventional programmer, does offer several unique benefits and follows in the footsteps of programs such as PCSail, the VPP written by faculty at the University of Michigan in the early 2000's. The yacht design program at Solent University, like many other naval architecture programs, is tailored around the use of excel as a computational tool, eschewing programming languages such as Python and MATLAB for tools that are more commonly used in the industrial field today. Thus, developing this VPP in the framework of Excel makes it more accessible to undergraduate students as well as naval architects and hobbyists for whom commercial off the shelf VPPs are prohibitively expensive. The design of Excel with its cell structure, vast library of nearly 500 functions, and capability for User Defined Functions are what have enticed naval architects and engineers and are precisely what enable this VPP to be transparent to the user, allowing

students to understand what is happening at each step and making it a functional teaching aide.

To determine hydrodynamic lift and drag forces, this VPP makes heavy use of equations derived from tow tank experiments conducted with the Delft Systematic Yacht Hull Series. This series is based off several parent hulls which have been systematically altered over a range of various parameters (such as their prismatic coefficient, length to beam ratio, etc.) to create a series of over 50 models. From extensive tow tank testing of these models in various conditions, regression lines have been fit to experimental data which model the different hullform's performance and allow for extrapolation to other hullforms. Originally developed in the 1970's the first parent hull was designed to be representative of contemporary sailboats. However, over the past 50 years, the design of sailboats has changed considerably warranting the creation of new parent hulls and extensions to the original systematic series. To verify the validity of using the trends derived from the Delft series on more modern style sailboats a Farr 52' model was tested at the Hydrodynamics Centre at Solent University. This model is outfitted with a fin keel with a bulb as is common in cruising and racing yachts today.

2 GENERAL THEORY OF SAILING

2.1 Wind Vectors

Sailboats are propelled through the water by the lift forces generated by their sails. An overhead view demonstrates that a properly trimmed and adjusted sail acts as an airfoil section with the angle of the wind correlating to the foil's angle of attack. Thus, the lift a sail (or set of sails) generates and the subsequent speed a given sailboat will sail at is primarily determined by the wind speed and angle. However, as the boat sails and is heeled by the wind the apparent wind speed and angle that the sails experience differ from the true wind speed and angle that an observer on dry land would note as illustrated in Figure 2.

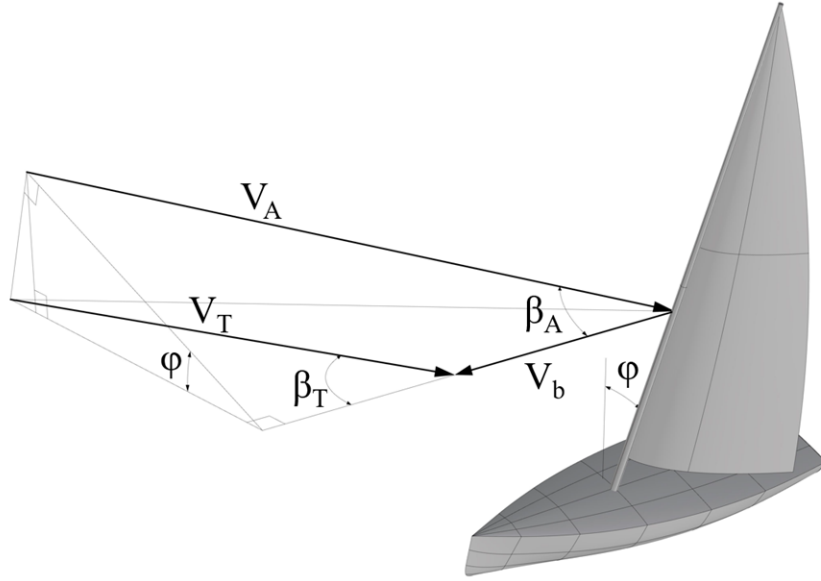


Figure 2: Wind speed and angles as experienced by a heeled sailboat

For an upright sailboat, apparent wind speed, V_A , is equal to the sum of the true wind speed and boat speed (V_T and V_b respectively), and the apparent wind angle β_A is $\tan^{-1} \left(\frac{V_T \sin \beta_T}{V_b + V_T \cos \beta_T} \right)$. When heeled at an angle ϕ the wind speed component incident to the chord of the sail decreases by a factor of $\cos \phi$. Thus, the apparent wind speed and angle that the sails experience when heeled can be described by the following equations.

$$V_A = \sqrt{(V_T \sin \beta_T \cos \phi)^2 + (V_b + V_T \cos \beta_T)^2}$$

$$\beta_A = \tan^{-1} \left(\frac{V_T \sin \beta_T \cos \phi}{V_b + V_T \cos \beta_T} \right)$$

The apparent wind acting on a sail with sail area SA generates a lifting force, L , normal to the sail plane which provides the main propulsive force for the sailboat as well as an aerodynamic drag force, D , parallel to the apparent wind.

$$L = \frac{1}{2} \rho_A C_L V_A^2 SA, \quad D = \frac{1}{2} \rho_A C_D V_A^2 SA$$

The total sail force a yacht experiences depends not just on apparent wind speed and sail area but also on the number of sails and any obstructions to them. Adding more sails to a yacht, in general, increases the sail area but can decrease the effectiveness of each sail as oncoming apparent wind is disturbed by windward sails. The actual coefficient of lift for a given sail is then the the coefficient of the sail with an undisturbed wind multiplied by the blanketing factor, Bl , a term that describes the reduction in lift of a given sail due to the presence of upwind sails which decrease apparent wind speed.

As a sailboat encounters stronger winds the forces on the sail further heel the vessel. Yacht designers have long understood this and oft used it to their advantage by creating hullforms whose waterline lengths increase and wetted surface areas decrease when inclined to expected wind heeling conditions as illustrated by the Farr 52' wetted surface area curve plotted in Figure 3. Wind conditions, however, are not always cooperative and heavy wind conditions (or overly large sail sets) can cause a yacht to heel excessively, increasing viscous drag and causing the boat to sail at a slower speed.

To combat excessive heel, sailors reef the sails to make them smaller reducing their lift generation and thus reducing heeling. Therefore, the sail area of a yacht is the area of the sails at maximum extent (the reference sail area) times the amount the sails are reefed where *Reef* is a value from 1.0, an unreefed sail, to 0, a sail that has been reefed to zero sail area (this is a hypothetical minimum, typically the value will no be less than 0.7 which equates to a sail area 49% of the original sail). It should be understood that the *Reef* parameter relates to the reduction in luff (the height of the sail along the mast) and not the total sail area directly, thus the effect of reefing an entire set of sails can be described as:

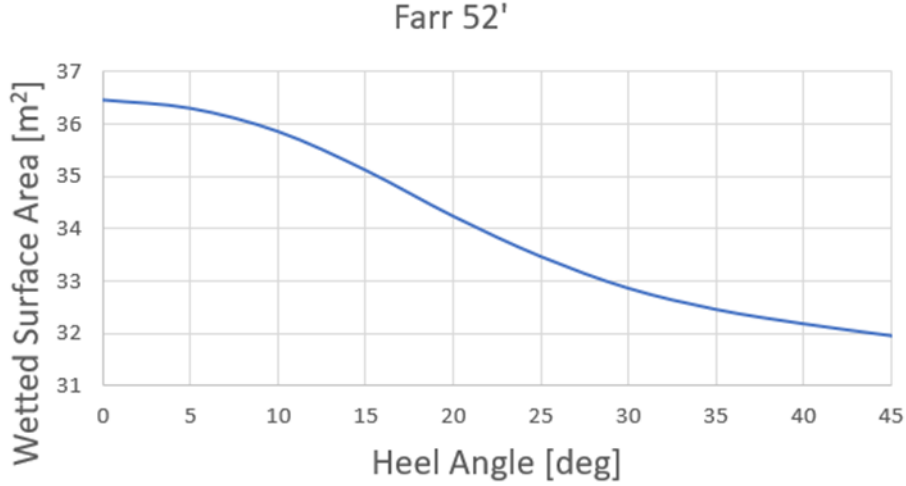


Figure 3: Wetted surface area versus heel angle for a Farr 52'

$$SA = Reef^2 \times SA_{Ref} \quad \longrightarrow \quad SA = Reef^2 \times \sum_{sails} SA_i$$

This equation makes two assumptions: that reefing the sails does not affect any parameters of the sail other than area and that all the sails are reefed together. The first assumption is a matter of seamanship and sail design which, when properly executed, enable a decrease in sail area while maintaining sail camber and twist and thus preserving the sail's coefficient of lift. The latter assumption of simultaneous reefing of sails preserves the longitudinal center of effort of the sail set and maintains a constant lead, that is, the distance from the center of effort of the sails to the underwater center of lateral resistance. When upright, the *CoE* is typically 3 – 4% forward of the *CLR* as when heeled the *CLR* moves forward due to changes in underwater geometry of the hullform resulting in a well balanced boat where the *CoE* is directly above the *CLR* (when heeled). While excessive wind load, sub-optimal wind conditions, or improper sail sets may induce undesirable yawing moments (such as weather helm and lee helm) warranting non-uniform reefing of sails these are fringe cases which are averaged out by the assumption of uniform reefing.

Sails, like all foils, generate lift through the creation of a pressure gradient, a process greatly aided by chord-wise camber. However, unlike rigid foils, the camber of a sail is in turn affected by the flow of air passing it. Sail designers manufacture sails with an appropriate amount of camber to maximize the efficiency of the sail; however, wind

conditions may warrant a reduction in camber, that is, a flattening of the sail, in order to optimize the lift generated. To account for this phenomenon a flattening function, $Flat$, is used to numerically modify the calculated lift generated by a sail. Typical values for this function range from 1.0, no flattening of the sail, to 0.5, indicating the camber is flattened such that it only generates half the original lift. The combination of $Reef$ and $Flat$ enable designers to model all the possible ways a sailor can trim sails in order to optimize the efficiency of a sail. Thus, the actual coefficient of lift for a given sail, $C_{L,Act}$, can be calculated as a function of the untrimmed coefficient of lift, $C_{L,0}$, and the blanketing, reefing, and flattening functions as:

$$C_{L,Act} = C_{L,0} \times Bl \times Reef^2 \times Flat$$

2.2 Sail Forces

The total lift generated by a given sail set can be calculated as the lift from an analogous single foil with the same sail area and coefficient of lift:

$$C_L = \frac{\sum_{sails} C_{L,i}(\beta_A) Bl_i SA_i}{SA_{tot}} \times Reef^2 \times Flat$$

where the total coefficient of lift for a given sail set is the average of the coefficients of lift from each individual sail weighted by sail area. Finally, the coefficients of lift for each individual sail can be found as a function of the type of sail and the apparent wind angle. After extensive testing the Offshore Racing Congress (ORC 2022) has proposed the lift coefficients presented in Figure 4 in their IMS (International Measurement System) Rule Book.

Calculation of drag on the sail sets is a bit more complicated owing to the different contributing sources. The coefficient of drag for a given sail can be decomposed into the parasitic drag, C_{DP} , describing viscous resistance due to air flow over the sail; quadratic profile drag, C_{DQ} , resulting from changes in the boundary layer due to lift generation; and induced drag, C_{DI} , stemming from the creation of vortices.

$$C_D = C_{DP} + C_{DQ} + C_{DI} \quad \text{with} \quad \begin{cases} C_{DQ} = k_q C_L^2 \\ C_{DI} = \frac{A}{\pi S^2} C_L^2 \end{cases}$$

For a complete set of sails, the coefficient of parasitic drag is a weighted average of the contribution of each sail, and, as a linear function of sail area, the parasitic drag of an

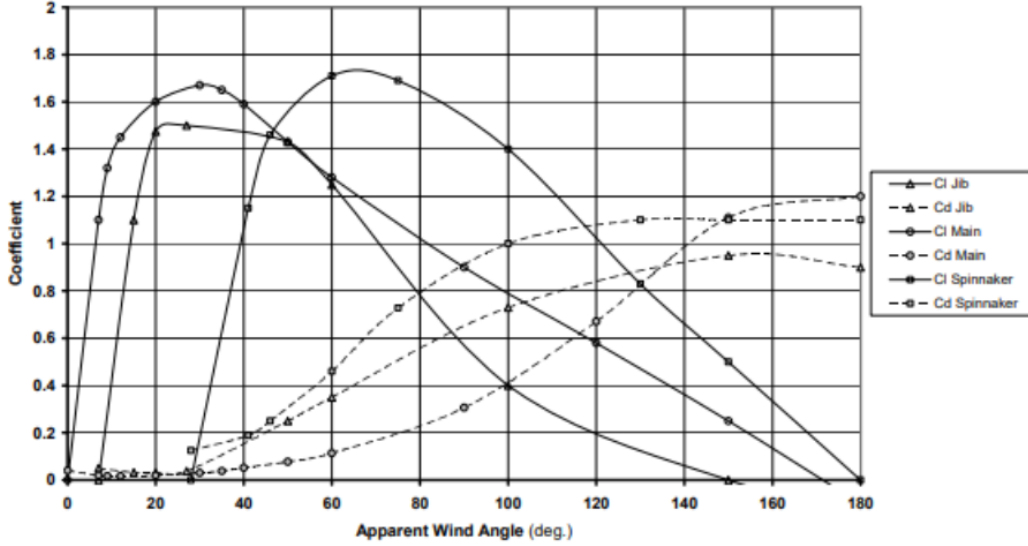


Figure 4: IMS sail lift and drag coefficients

adjusted sail is simply that of the full sail multiplied by the reefing factor squared. Notably, there is no flattener term included as adjusting the camber of a sail does not impact surface area. C_{DP} values are typically derived from the drag forces parallel to the apparent wind measured on sails during wind tunnel testing; a standard approximation for these values for different sails is given in Figure 4.

The quadratic profile drag, which is the viscous resistance due to changes in the boundary layer caused by lift is proportional to the coefficient of lift squared, $C_{DQ} = k_q C_L^2$, where k_q is the quadratic profile drag coefficient for a given sail type. Typically, designers use 0.09 as a standard value for the k_q factor (Barkley, personal communication). As C_{DQ} is proportional to C_L^2 , reefing and flattening the sail set adjusts the quadratic profile drag by a factor of $(Reef^2 \times Flat)^2$.

Lift on a sail is generated by a difference in pressure created by flow past the wing shaped foil. At the edges of the sail, this pressure difference must be zero which causes some of the wind to curl from the high pressure side to the low pressure side, creating vortices, and resulting in induced drag. Thus, C_{DI} must a function of the sail area, the span, and the coefficient of lift of a given sail. Further, trimming the sail means that induced drag is also reduced by a factor of $(Reef^2 \times Flat)^2$.

Therefore, the total coefficient drag of the sail set, taking into account reefing and flattening, is described as:

$$C_D = C_{DP} + C_{DQ} + C_{DI} \quad \text{with} \quad \begin{cases} C_{DP} = \left(\frac{\sum C_{DP,i} A_i B_i}{A_{Ref}} \right) \times Reef^2 \\ C_{DQ} = \left(\frac{\sum k_{q,i} A_i B_i C_{L,i}}{A_{Ref} C_{L,i}} \right) C_L^2 \times (Reef^2 \times Flat)^2 \\ C_{DI} = \frac{A}{\pi S^2} C_L^2 \times (Reef^2 \times Flat)^2 \end{cases}$$

3 VPP GOVERNING EQUATIONS

For a three degree of freedom VPP, six forces and moments are sufficient to describe ship motion, namely resistance, drive force, sail side force, keel side force, righting moment, and heeling moment. Balancing each pair of forces and moments results in a a sailboat that is in equilibrium with respect to surge, sway, and roll. Fundamentally, a VPP works by determining which combinations of leeway, velocity, and heel angle satisfy these conditions so that this vessel is in dynamic equilibrium. The following section describes how these forces and moments experienced by a yacht are calculated. Further details are provided in Appendices 8.4 and 8.5.

3.1 Resistance and Powering

3.1.1 Resistance

For power driven vessels, in general, their upright resistance is sufficient to determine powering requirements. However, this assumption cannot be made for sailing vessels which are expected to sail at a significant heel angle. As previously discussed, heeling a sailboat changes both the underwater volume and wetted surface area, inherently altering the resistance that the boat encounters. As the underwater volume changes asymmetrically it it generates an angle of attack with respect to oncoming water flow thus also creating induced drag. Therefore, the total resistance that a heeled sailboat experiences can be decomposed as the sum of the upright resistance, R_U ; change in resistance due to heeling, R_H ; and induced drag, R_I ; or:

$$R_{Tot} = R_U + R_H + R_I$$

Upright Resistance

The upright resistance of any vessel can be decomposed into two components: viscous resistance and residuary resistance. Viscous resistance, R_v , is the drag due to skin friction of the hull as well as the shape of the hullform while residuary resistance, R_r , is the remaining resistance. In their method for estimating hull resistance on the Delft Systematic Yacht Hull Series (DSYHS), Gerritsma, Onnick, and Versluis 1981 deviate from this

practice by decomposing the total upright resistance into a purely frictional component and a residuary one which includes the effects of the form factor.

$$R_U = R_v + R_r = R_f(1 + k) + R_r \xrightarrow{\text{Gerritsma}} R_U = R_f + R_{r+FormFactor}$$

By decomposing the total resistance in this manner, the modified residuary resistance could be calculated by subtracting the skin friction resistance from the total resistance of the DSYHS models determined during tow tank testing. From there Gerritsma and his colleagues were able to develop an equation that modeled the residuary resistance data. The frictional resistance of any vessel can be found using the following equation and the International Tow Tank Conference 1957 friction line coefficient.

$$R_f = \frac{1}{2} \rho V_b^2 S_c C_f \quad \text{where} \quad C_f = \frac{0.075}{(\log R_e - 2)^2}$$

Notably, for the calculation of the Reynolds' number Gerritsma defines the characteristic length of the hull as 70% of the waterline length in order to take into account the profile and waterline slope of sailing yachts (Gerritsma, Onnick, and Versluis 1981). Further, Keuning and Sonnenberg 1999 demonstrated that the wetted surface area of the DSYHS hulls can be found as a regression line with respect to principle characteristics as:

$$S_c = \left(1.97 - 0.171 \frac{B_{WL}}{T_c}\right) \left(\frac{0.65}{C_m}\right)^{\frac{1}{3}} (\nabla_c L_{WL})^{\frac{1}{2}}$$

For the Farr 52', this wetted surface estimate only deviates from the actual value by 0.73%. Thus, even though the Farr 52' has a different hullform compared to Delft series hulls, the wetted surface area approximation is still accurate as the hull is within the Delft series hull parameters.

From tank tests carried out with the Delft series bare hulls, that is canoe bodies without any appendages, Gerritsma's successors (Keuning and Sonnenberg 1999) were able to determine an empirical equation to estimate residuary resistance across series of hullforms based on various hull parameters of the form:

$$R_r = \nabla_c \rho g C_{r,c}$$

where

$$C_{r,c} = a_0 \left(a_1 \frac{LCB}{L_{WL}} + a_2 C_p + a_3 \frac{\nabla_c^{\frac{2}{3}}}{A_W} + a_4 \frac{B_{WL}}{L_{WL}} \right) \frac{\nabla_c^{\frac{1}{3}}}{L_{WL}} \\ + \left(a_5 \frac{\nabla_c^{\frac{2}{3}}}{S_C} + a_6 \frac{LCB}{LCF} + a_7 \left(\frac{LCB}{LCF} \right)^2 + a_8 C_p^2 \right) \frac{\nabla_c^{\frac{1}{3}}}{L_{WL}}$$

Values for coefficients a_0 to a_8 for Froude numbers 0.1 to 0.6 can be found in Table 9 of Appendix 8.5.1. This reformulation of R_U allows one to implicitly calculate the hull form factor when determining the residuary resistance. By not explicitly requiring the form factor this method is thus well suited for other hull forms with unknown form factors and is particularly useful early in the design cycle of a yacht.

The resistance of the appendages can likewise be decomposed into viscous and residuary components. However, for simpler geometries, such as fin keels and bulbs, there exist analytic expressions for the form factors such as those derived by Hoerner 1965:

$$(1+k) = \begin{cases} 1 + 2\frac{t}{c} + 60 \left(\frac{t}{c}\right)^4 & \text{for fins} \\ 1 + 1.5\frac{t}{c} & \text{for bulbs} \end{cases}$$

Thus, the total upright resistance, including keels and rudder appendages, can be written as:

$$R_U = R_f + R_r = \frac{1}{2} \rho V_b (S_c C_{f,c} + S_k C_{f,k} (1+k_k) + S_r C_{f,r} (1+k_r)) + \rho g (\nabla_c C_{r,c} + \nabla_k C_{r,k})$$

In this formulation rudders are assumed to be submerged deep enough so as not to influence wave making and thus there is no residuary component of resistance associated with rudders. There had been some debate on the influence of keels on residuary resistance, however, J.A. Keuning and U.B. Sonnenberg, in their synthesis and extension of the DSYHS tested different keels on various models and found the following relationship between keels and residuary resistance:

$$C_{r,k} = A_0 + A_1 \frac{T}{B_{WL}} + A_2 \frac{T_c + Z_{cbk}}{\nabla_k^{\frac{1}{3}}} + A_3 \frac{\nabla_c}{\nabla_k}$$

with coefficients A_0 through A_3 listed in Appendix 8.5.1 Table 10 for Froude number 0.2 to 0.6.

Heeled Resistance

Unlike most other types of vessels, sailboats are designed to sail while subjected to a significant heeling force; therefore, calculating upright resistance is not sufficient to determine the total drag on the vessel. The resistance of a yacht sailing while heeled (R_ϕ) can be decomposed into three components: upright resistance, R_U ; resistance due to heeling, R_H ; and induced resistance, R_I .

$$R_\phi = R_U + R_H + R_I, \quad \text{where} \quad R_H = \Delta R_v + \Delta R_r$$

The resistance due to heeling term is the sum of the changes in frictional and residuary resistance as the boat is heeled. The change in frictional resistance is simply due to the change in the wetted surface area where the heeled wetted surface area which can be calculated as:

$$S_{c,\phi} = S_c \left(1 + \frac{1}{100} \left(s_0 + s_1 \frac{B_{WL}}{T_c} + s_2 \left(\frac{B_{WL}}{T_c} \right)^2 + s_3 C_m \right) \right)$$

Again, Keuning and Sonnenberg 1999 provide values for these coefficient (s_0 to s_3) which are listed in Table 11 in Appendix 8.5.2. This formulation allows the change in frictional resistance due to heeling to be calculated as:

$$\Delta R_f = \frac{1}{2} \rho V_b^2 (S_{c,\phi} - S_c) C_f$$

Figure 5 illustrates the differences between this approximation of the heeled wetted surface area and the actual values from 0 to 35 degrees of heel for the Farr 52' hull. It can be clearly seen that the $S_{c,\phi}$ formulation well approximates the actual wetted surface area with the error being 1% or less for angles of heel up to 20 degrees. Notably, between 5 and 15 degrees, the range of heel angles the sailboat is most often expected to sail at, the error is the least. While the error does continue to increase after 20 degrees, it remains small and is exaggerated by the vertical axis. In all, these minor differences lend credence to change in frictional resistance formulation.

The change in residuary resistance due to heeling, which includes changes in wave making and form factors, must include the changes due to heeling the canoe body hull as well

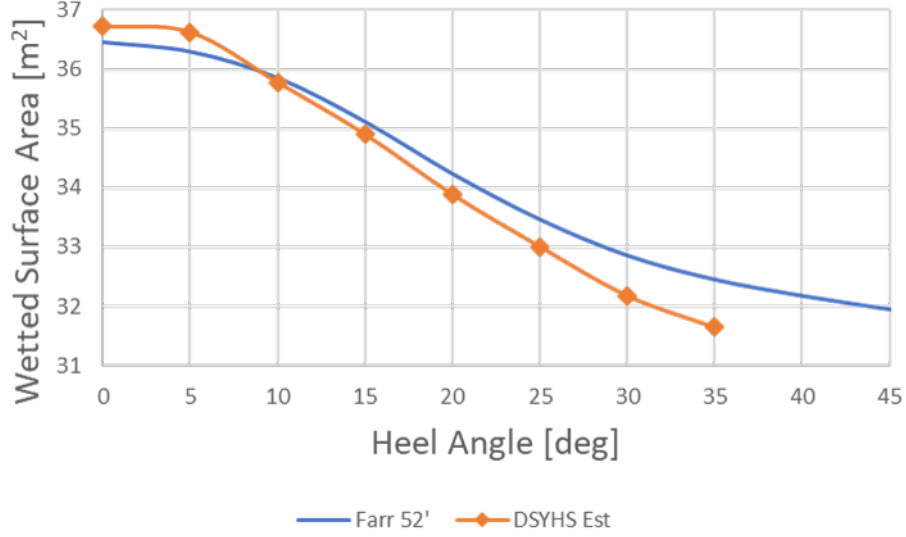


Figure 5: Wetted surface area comparison

as the keel. Again, Keuning and Sonnenberg 1999 demonstrate that for the effects of the bare hull, the residuary resistance for an arbitrary heel angle can be calculated by extrapolating from the $\phi = 20$ case (with ϕ in radians):

$$\Delta R_{r,h} = \Delta R_{r,h,\phi=20} 6.0\phi^{1.7}$$

The residuary resistance of the hull heeled to 20 degrees can be computed as the following equation with coefficients u_0 through u_5 documented in Appendix 8.5.3 Table 12:

$$\Delta R_{r,h,\phi=20} = \nabla_c \rho g \left(u_0 + u_1 \frac{L_{WL}}{B_{WL}} + u_2 \frac{B_{WL}}{T_c} + u_3 \left(\frac{B_{WL}}{T_c} \right)^2 + u_4 LCB + u_5 LCB^2 \right)$$

As a sailboat heels, its keel is brought closer to the surface, increasing its influence on wavemaking resistance. Thus, the degree to which heeling affects keel residuary resistance will primarily depend on the beam to draft ratio of the hull as well as the relative submergence of the keel with secondary influence from the wave making of the hull itself (length displacement ratio term). Combined, these three factors are themselves impacted by the speed of the boat and the angle of heel; thus, the change in residuary resistance due to heeling the keel is:

$$\Delta R_{r,k} = \nabla_k \rho g (ChFn^2\phi)$$

$$Ch = H_1 \frac{T_c}{T} + H_2 \frac{B_{WL}}{T_c} + H_3 \frac{T_c}{T} \frac{B_{WL}}{T_c} + H_4 \frac{L_{WL}}{\nabla_c^{\frac{1}{3}}}$$

Ch can be calculated with the values listed in Table 13 within Appendix 8.5.3.

Induced Resistance

As a boat yaws, its underwater volume and, more importantly, keel develop and angle of attack relative to the motion of the vessel and creates a lateral lifting force. This resultant side force also induces drag.

$$R_I = \frac{1}{2} \rho V_b^2 C_{Di} A_{Lat}, \quad \text{where} \quad C_{Di} = \frac{C_L^2}{\pi AR_e} \quad \longrightarrow \quad R_I = \frac{F_H^2}{\pi AR_e \frac{1}{2} \rho V_b^2 S_c}$$

Where F_H is the side force generated and AR_e is the total effective aspect ratio of the keel and hull. If the effective draft is defined as $T_e = \sqrt{AR_e S_c}$ then induced resistance is:

$$R_I = \frac{F_H^2}{\pi T_e^2 \frac{1}{2} \rho V^2}$$

Gerritsma, Keuning, and Onnick November 1992 offer the following formula to determine the effective draft of the combined hull-keel structure with coefficient values provided by Keuning and Sonnenberg 1999 (listed in Appendix 8.5.4, Table 14).

$$T_e = T \left(A_1 \frac{T_c}{T} + A_2 \left(\frac{T_c}{T} \right)^2 + A_3 \frac{B_{WL}}{T_c} + A_4 T_R \right) (B_0 + B_1 F_n)$$

Total Resistance

In summary, combining the previously discussed terms the total resistance of a yacht sailing while heeled and yawed is:

$$R_{Tot} = R_U + R_H + R_I$$

3.1.2 Powering (Sail Drive Force)

The drive force which propels the sailboat through the water is the resultant aerodynamic force resolved along V_b , the velocity of the boat, and can be calculated with respect to

generated lift and drag. Figure 6, provided by Professor Barkley, illustrates this relationship (though notably he uses λ to represent the leeway angle).

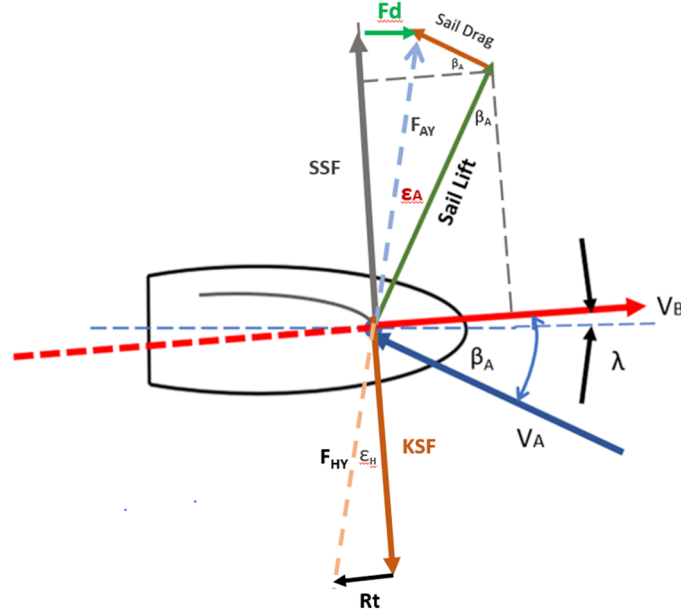


Figure 6: Plan view of keel and sail forces

From Figure 6 it is clear that the drive force can be written as:

$$F_D = L \sin \beta_A - D \cos \beta_A$$

where β_A is the apparent wind angle when heeled. As most sailing vessels have more than one sail, the lift generated by an entire sail set can be calculated as a summation of the contribution of each individual sail scaled by the areas of the sails.

$$L = \frac{1}{2} \rho_A V_A^2 (SA \times C_L) \quad \text{where} \quad C_L = \frac{\sum_{sails} (SA_i \times C_{L,i})}{SA_{Tot}} \times \text{Blanketing} \times \text{Reef}^2 \times \text{Flat}$$

3.2 Side Forces

3.2.1 Sail Side Force

As the sails on a sailboat experience apparent wind the aerodynamic lift and drag forces create a resultant force with components parallel to the ship's motion and perpendicular to it. The parallel component, as previously discussed, is the sail drive force which propels

the boat forwards. The perpendicular component, the sail side force, is the force inducing lateral motion and similarly referencing Figure 6 it can be calculated as:

$$SSF = L \cos \beta_A + D \sin \beta_A$$

where the lift generated by the sails is calculated as:

$$L = \frac{1}{2} \rho_A V_A^2 S_A \times C_L$$

3.2.2 Keel Side Force

In order to prevent the sailboat from accelerating laterally the sail side force must be balanced by an equal keel side force. In much the same way that the sail set acts as a vertical foil, so too does the underwater volume of a yacht act as a foil and generate lift with parallel and perpendicular components. As the boat heels, so to does the heeling force, F_H , reducing the side force by a factor of $\cos \phi$ so that the keel side force parallel to the water line is:

$$KSF = F_H \cos \phi$$

The heeling force generated by the hull and keel is the result of the lift created by their foil shaped cross-sections travelling at an angle of attack, β , due to the leeway of the sailboat. For small angles of attack, the change in lift generated by a foil varies linearly with the change in angle of attack. With this in mind, the heeling force can be written in terms of the lift slope curve, leeway, heel, and dynamic pressure as:

$$KSF = \frac{1}{2} \rho V_b^2 S_c \times C_L \quad \longrightarrow \quad F_H = \frac{\partial C_L}{\partial \beta} \times \frac{\beta \frac{1}{2} \rho V_b^2 S_c}{\cos \phi}$$

From experimental observations, Gerritsma, Keuning, and Onnick 1993 were able to develop a least squares regression that calculates the heeling force in terms of $\frac{T^2}{S_c}$ and $\frac{T_c}{T}$ which, in effect, describe the effective aspect ratio of the underwater hull. Values for coefficients b_1 through b_4 are tabulated in Appendix 8.5.5 Table 15 for heel angles of 0, 10, 20, and 30 degrees.

$$\frac{\partial C_L}{\partial \beta} = b_1 \frac{T^2}{S_c} + b_2 \left(\frac{T^2}{S_c} \right)^2 + b_3 \frac{T_c}{T} + b_4 \frac{T_c}{T} \frac{T^2}{S_c}$$

Thus, the lateral keel side force that the yacht experiences at a give heel and leeway angle can be succinctly (though at the expense of symbolic intuition) expressed as:

$$KSF = \beta \frac{1}{2} \rho V_b^2 \left[b_1 T^2 + b_2 \frac{T^4}{S_c} + b_3 \frac{T_c}{T \times S_c} + b_4 T_c \times T \right]$$

3.3 Righting and Heeling Moments

3.3.1 Righting Moment

As a boat heels its center of buoyancy typically shifts laterally due to changes in geometry of the displaced volume of water leading to a mismatch in the positions of the transverse centers of gravity and buoyancy. The eccentric loading of the weight of the ship and its buoyancy create a righting moment, RM , that seeks to restore the vessel to it's upright condition (assuming a positive righting arm). For small angles of heel, this moment can be described in terms of the the metacentric height, GM , which remains relatively stationary:

$$RM = GZ \Delta g, \quad GZ = GM \sin \phi \cos \phi$$

However, it is not uncommon for yachts to sail heeled to angles greater than 25 degrees, well beyond the scope of small angle approximations. Therefore, a slightly modified approach is adopted where a residual stability lever, ZZ' , is added to the standard righting arm lever as illustrated in Figure 7.

The modified righting arm lever is then GZ plus the residual stability lever. Towing the DSYHS models at various angles of heel, Gerritsma, Onnick, and Versluis 1981 were able to ascertain righting moments for each model and using a least squares fit method and derived the following equation where the first term expresses the influence of forward speed, the second term represents the non-linearity for greater heel angles, and L_{WL} is included to properly scale the data (the original data set was normalized by L_{WL}):

$$ZZ' = MN \sin \phi = L_{WL} (D_2 \phi F n + D_3 \phi^2)$$

with ϕ in radians and the coefficients D_2 and D_3 determined as:

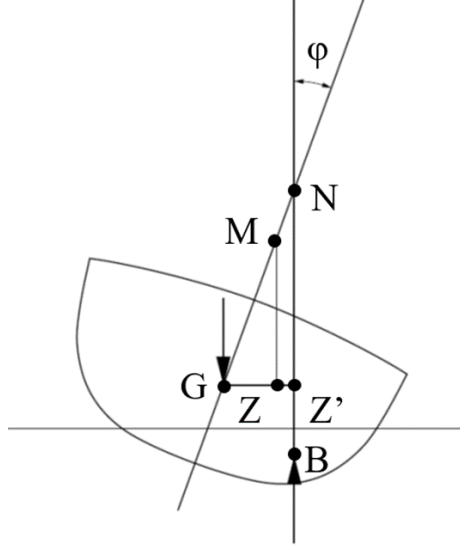


Figure 7: Definition of residuary stability

$$\begin{cases} D_2 = -0.0406 + 0.0109 \left(\frac{B_{WL}}{T_c} \right) - 0.00105 \left(\frac{B_{WL}}{T_c} \right)^2 \\ D_3 = 0.0636 - 0.0196 \left(\frac{B_{WL}}{T_c} \right) \end{cases}$$

The metacentric height of a vessel, GM , is defined as the vertical center of buoyancy plus the metacentric radius minus the vertical center of gravity.

$$GM = KM - KG = KB + BM - KG$$

While the center of gravity of a yacht remains relatively constant with respect to heeling (assuming there are negligible amounts of liquids on board and the weight of the crew is small compared to the displacement of the vessel), the center of buoyancy and metacentric radius can vary greatly. Once again, using a least squares fit, Gerritsma and his colleagues were able to determine the following fit line to calculate KM :

$$KM = 0.664T_c + 0.111 \frac{B_{WL}^2}{T_c}$$

Noticeably, the first term indicates that the vertical center of buoyancy, KB , is approximately two thirds the canoe body draft. This value is intuitively reasonable assuming an underwater volume that mimics a triangular prism.

The second term represents the metacentric radius, BM . The standard calculation for the metacentric radius of a vessel divides the second moment of area of the waterplane

area, I , by the displaced volume.

$$BM = \frac{I}{\nabla} \quad \begin{cases} I = \frac{1}{12}b^3l & I_{rectangle} \\ I = \frac{\pi}{64}b^3l & I_{ellipse} \\ I = \frac{1}{48}b^3l & I_{triangle} \end{cases}$$

Assuming an elliptical waterplane area and remembering that the displaced volume is equal to $B_{WL} \times L_{WL} \times T_c \times C_b$ leads to the following calculation of BM :

$$BM_{ellipse} = \frac{\frac{\pi}{64}b^3l}{\nabla} = \frac{\frac{\pi}{64}B_{WL}^2}{C_b T_c} \quad \longrightarrow \quad 0.111 = \frac{\pi}{64C_b}, \quad C_b \approx 0.44$$

Then, calculating the block coefficient from the BM equation yields an approximate value of 0.44, which is well within the accepted range of sailing yacht block coefficients, validates Gerritsma's 0.111 coefficient in his BM calculation.

With these formulations, the righting moment of a sailing yacht is expressed as a function of Δ , L_{WL} , B_{WL} , T_c , KG , Fn , and ϕ ; hull parameters readily known even at the outset of a project.

3.3.2 Heeling Moment

As the sail side force acts above the center of rotation of a sailboat, a heeling moment is created. While it is difficult to pinpoint where exactly the vessel is heeling about, the upsetting moment can be resolved by multiplying sail side force (which acts as the heeling force) by the heeling lever arm which has been decomposed into two components: the center of effort of the sails, Ze , and the center of lateral resistance of the hull, CLR .

$$HM = SSF \times (Ze + CLR)$$

The center of effort of the total sail set is the average of centers of effort of each individual sail weighted by the force applied. As the dynamic pressures cancel out the weighting factor is the product of the sail area, blanketing factor, and coefficient of resultant force (that is, the norm of the coefficients of lift and drag).

$$Ze = \frac{\sum Ze_i SA_i B_i \sqrt{C_{L,i}^2 + C_{DP,i}^2}}{SA \sqrt{C_L^2 + C_{DP}^2}}$$

The distance between the center lateral resistance and the waterline for the DSYHS is well approximated by the following expression (Gerritsma, Onnick, and Versluis 1981):

$$CLR = D_4 T, \quad \text{where } D_4 = 0.414 - 0.165 \frac{T_c}{T}$$

4 THREE DEGREE OF FREEDOM VPP

The previously discussed six forces and moments that describe the response of a sailboat to various environmental conditions theoretically are sufficient to develop a three degree of freedom VPP.

In order for the sailboat to be in equilibrium the aerodynamic forces must be balanced by equal hydrodynamic forces. Assuming that the sailboat is travelling at a constant speed the drive force, F_D , resulting from the generated lift and drag resolved along the ship's heading is equal in magnitude to the resistance of the sailboat. Likewise, the lateral side force component of the sail forces must be equal to the hydrodynamic side forces of the lift generated by flow past the underwater hullform and keel. Similarly, for the sailboat to be in equilibrium the heeling moment induced by the eccentric wind loading (applied at the center of effort of the sails) must be balanced by an equal righting moment generated by the underwater volume of the hull. These three equilibria are the foundations of a three degree of freedom VPP and once satisfied they describe the expected behavior of a sailboat. While each of the previously discussed equations are individually easy to solve they rely on the results of other equations resulting in a complex system of equations. For example, the total resistance of a yacht is dependant on its boat speed which is in turn a function of the drive force. Thus, determining the behavior of a vessel in any given wind condition requires solving a complex, non-linear, system of equations.

The goal of a 3 DoF VPP is to calculate the speed, leeway, and heel angle that a yacht can be expected to experience for a given true wind speed and true wind angle combination. From the previous section it is evident that all of the governing equations are inextricably linked, however, it is clear that their influences on the different degrees of freedom are not equal.

4.1 Optimization Problem

The solution to the speed, heel, and leeway of a boat for a given true wind speed and angle can be approximated by reformulating this non-linear combination of equations as

an optimization problem. In order to satisfy equilibrium conditions for all the degrees of freedom opposing forces must be equal which is computationally equivalent to saying the difference between opposing forces must be zero.

$$\begin{cases} R_T = F_D \\ KSF = SSF \\ RM = HM \end{cases} \quad \longrightarrow \quad \begin{cases} |R_T - F_D| \leq \varepsilon_D \\ |KSF - SSF| \leq \varepsilon_{SF} \\ |RM - HM| \leq \varepsilon_M \end{cases} \quad \text{where } \varepsilon_i \ll 1$$

If instead of of these three equilibrium conditions equaling zero they are less than or equal to arbitrarily small residual values, ε_i , then they become optimization problems wherein they can be treated as objective functions. That is, by minimizing any of the given residuals that equilibrium condition is satisfied. Since the residuals must be strictly positive, all three of the equilibria can be considered satisfied when the sum of the residuals is minimized (and arbitrarily close to zero), or more concisely:

$$\arg \min_{V_b, \beta, \phi} \sum \varepsilon_i$$

In other words, the V_b , β , and ϕ values that minimize the differences between opposing forces are the boat speed, leeway angle, and heel, respectively, for a given true wind condition. Since the orders of magnitude of the forces differ greatly, in order to preserve equal weighting of each equilibrium condition their residuals are actually defined as the percentage difference between opposing forces (for example: $\frac{|R_T - F_D|}{R_T} \leq \varepsilon_D$).

4.2 Implementation

Excel's workbook/worksheet structure allows for a neatly organized implementation of the governing equations and optimization; the first two worksheets are dedicated to the collection and processing of input parameters, next there is a dashboard worksheet that displays calculated results, and then there are follow on work sheets dedicated to computing resistance and powering, side forces, and moments (heeling and righting). Since the goal of this VPP is to determine the speed of a sailboat across a range of true wind speeds and angles each row is dedicated to a unique combination of V_T and β_T . Within the results dashboard worksheet, after columns detailing the wind conditions, there are columns for leeway, boat speed, and heel angle, as well as for each equilibrium pair (KSF

and SSF ; R_T and F_D ; and RM and HM) which call data from their respective computational worksheets. Finally, there are columns dedicated to the residual value between each equilibrium pair and a summation of those residuals in the furthest right column.

Conveniently, there is an Excel add-in program, Solver, that can be used to find optimal values (minima and maxima) for a formula subject to various constraints. By setting the sum of the residuals for a given row as the objective function and the degrees of freedom cells as decision variables, Excel is able to determine which combination of values of leeway, speed, and heel result in the smallest differences between equilibrium values. These values are subject to various constraints that bound the feasible region of where the solution can be found. The Froude number is constrained to values between 0.1 and 0.6 (inclusive) as those are the minimum and maximum speeds that the Delft series yachts were tested at and tabulated values for regression coefficients do not extend past those limits. Similarly, the Delft series models were only heeled to 30 degrees which limits the potential heel value in the VPP from 0 to 30 degrees. Leeway is constrained between 0 and 10 degrees as anything beyond those values are physically unreasonable. While the tabulated values for regression coefficients are discrete, intermediary values can be found through linear interpolation of neighboring values (further detailed in Appendix 8.7.3). However, the tabulated values do not necessarily exhibit trends that allow for extrapolation of these values beyond the tested values with any level of confidence.

Manually conducting this operation for one or two wind conditions is acceptable, however, given the several dozen wind conditions required to properly evaluate sailing performance this method becomes rather cumbersome and time consuming. Instead, a Macro is utilized that automatically loops through every wind condition. This automation has the added benefit of also allowing for greater functionality in the optimization process. For example, due to the complex, non-linear nature of this optimization problem, occasionally Solver is unable to find the global minimum (which should be close to zero) and instead finds a local minimum stopping iteration. To combat this for any wind condition where the sum of the residuals is greater than 0.05 (that is a total difference in equilibrium forces of 0.05%) the macro determines which degree of freedom has the greatest residual, replaces the respective decision variable with a value interpolated from neighboring wind condi-

tions (that is, wind conditions with the same wind angle but different wind speeds), and re-initiates the optimization loop for that wind condition.

In essence, this second procedure has the effect of re-initializing the optimization loop with more satisfactory initial conditions, increasing the likelihood of finding the global minimum and decreasing the number of iteration steps as the starting point it typically closer to the solution. A more indepth description of how this macro works in explained in Appendix 8.8.

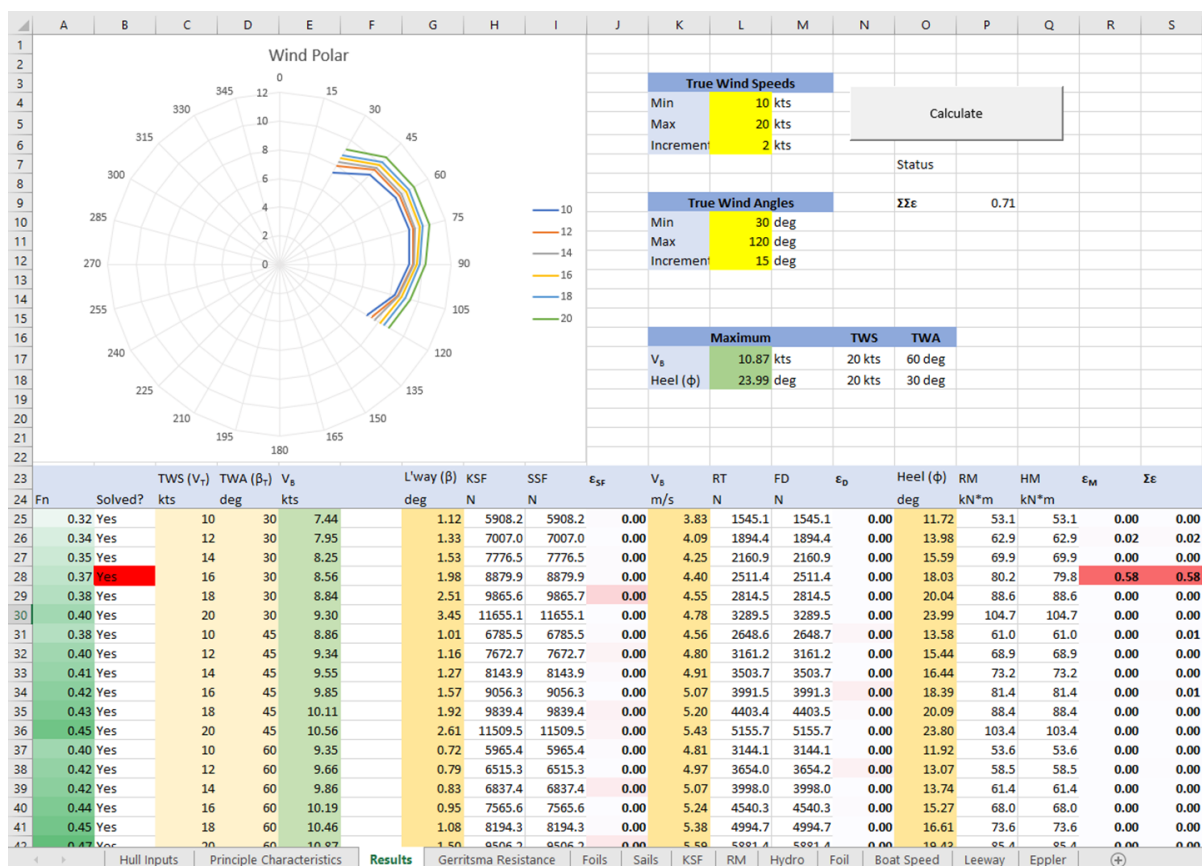


Figure 8: VPP Dashboard

4.3 Validation

To validate this VPP it was run analyzing the full scale Farr 52' hull parameters and sail set and the computed results were compared to those from WinDesign VPP. WinDesign VPP is a three degree of freedom velocity prediction program produced by the Wolfson Unit at the University of Southampton. Though specifics on how it works are not publicly

available it is based on IMS coefficients and was simulations conducted utilized its Delft mode (and thus should give similar results).

4.3.1 Direct Experimental Method

In order to properly calculate boat speed WinDesign VPP requires the user to input sail parameters, hull parameters, and appendage dimensions. Since WinDesign VPP is intended for all stages of the design process as a default it makes various assumptions which are valid for the majority of yachts but may not perfectly model a specific boat. Therefore, the designers enable users to overwrite many of these assumptions with experimental data, most notably the effective span of the keel and resulting side force. To overcome the complexity of the contributions of the hull and keel, as well as their shapes, angles of attack, and effect of heeling, the program simplifies the side force calculation by estimating an effective draft for the keel which approximates the side force that the vessel experiences.

As the side force generated by a yacht's keel is a function of boat speed, heel angle, and leeway; WinDesign VPP is able to interpolate keel side force through regressions of given experimental data points. When a boat experiences a leeway angle, the keel and underwater hull volume develop an angle of attack creating an additional resistance component: induced resistance. For small angles of attack, there is a linear relationship between total resistance and side force squared; therefore, by testing a model at different leeway angles (but same speed) one can develop a regression line to determine the total resistance as a function of side force squared as seen in Figure 9.

By determining the slope and y-axis intercept of the resistance versus side force squared relationship at different heel angles and speeds WinDesign VPP then has a complete data set from which it can interpolate the expected side force for any given combination of sailing conditions (within the three degree of freedom construct). Further, the program calculates side force as a function of leeway angle:

$$SF = AL_0 + AL_s\beta \quad \text{where} \quad AL = \frac{L}{q} = \frac{L}{\frac{1}{2}\rho V_b^2}$$

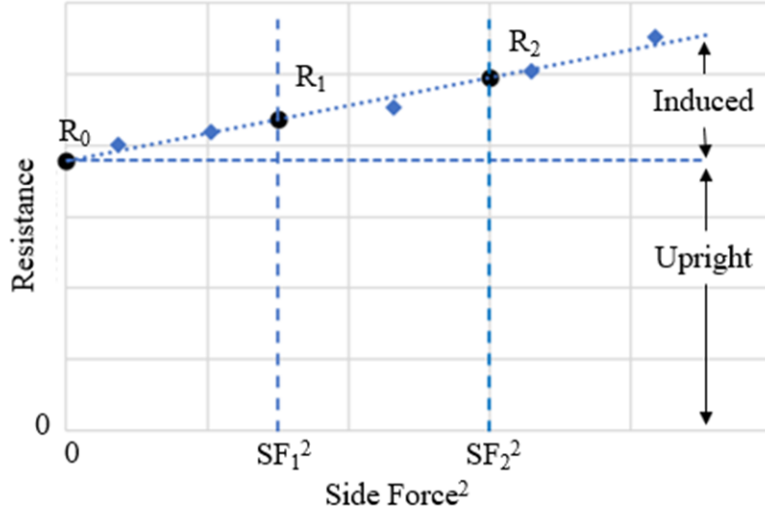


Figure 9: Relationship between resistance and side force (from leeway experiments)

In this formulation AL_0 is the lift area at zero leeway and AL_s is the lift area with respect to yaw, both of which represent the lateral projected area that the side force is acting on. Thus, to calculate the total resistance in all conditions WinDesign VPP requires values for the upright resistance, R_0 , resistance at two distinct side forces, R_1 and R_2 , the lift area at zero leeway, AL_0 , and the lift area slope, AL_s , all across a range of speeds and heel angles in addition to the upright resistance versus speed curve.

Parameter	Farr 52	
L_{OA}	2.2642	m
L_{WL}	2.0853	m
B_{WL}	0.4886	m
T_c	0.07	m
∇_c	0.029012	m ³
C_p	0.536	–
LCB	55.59	%
S_c	0.7831	m ²

Table 1: Farr 52' hull parameter summary

To obtain the requisite data points, a 2 meter Farr 52' model (whose principle characteristics are listed in Table 1) was tested in the towing tank at the Solent University

Hydrodynamics Centre. The model was first tested in the upright position across a range of speeds correlating to Froude numbers between 0.15 and 0.65. Next, while still in the upright position, the model was tested over a range of five leeway angles (1.5, 2.5, 4, 5, and 6 degrees) and five Froude numbers (0.28, 0.31, 0.35, 0.39, and 0.42). The experimental results were scaled from model to ship dimensions using the ITTC 1978 method by decomposing the results into viscous and residuary components. The viscous friction was further decomposed by source: hull, keel, and keel bulb. Since these three sources all have different characteristic lengths, their viscous drag contributions must be calculated separately using the ITTC 1957 Friction Coefficient Line. Summing up these three contributions and subtracting from the total experimental resistance results in the residuary resistance. With the experimental results fully decomposed into constituent parts, they can then be scaled to full size. The viscous components are each individually scaled by recalculating their contributions according to the ITTC 1957 Friction Coefficient Line using their respective full scale Reynolds' numbers. The residuary resistance is scaled geometrically by the scaling factor cubed (and multiplying by 1.025 since the experiments were conducted in fresh water but the boat is expected to sail in salt water). Combining all these resistance components results in the total resistance of the full sized yacht. As with the residuary resistance, the measured side force scales geometrically by the scaling factor cubed (and the 1.025 salt water multiplier).

With the model resistance and side force scaled to the full sized ship, the WinDesign VPP Direct Experimental inputs can be calculated. For each series of test runs conducted at the same heel angle and speed but varying leeway angles, plotting the resistance versus side force squared produces a series of points that can be well approximated by a linear regression line. The y-intercept of this regression line is the R_0 value, that is, the yacht's resistance without induced drag stemming from leeway angle (since there is no side force acting on the vessel). Next, two other side force squared values are chosen, in this case 150 and 300 kN^2 , and their respective resistances are determined through multiplying the side force squared value by the slope of the trend line and adding R_0 as graphically demonstrated in Figure 9. Remembering that dynamic pressure, q , is calculated as $\frac{1}{2}\rho V_b^2$, then $\frac{F_H}{q}$ can be determined for each run by dividing the side force by the dynamic pressure. Once again, plotting $\frac{F_H}{q}$ versus leeway angle (in radians) results in a nearly straight line.

The y-intercept of the regression line is the AL_0 value and the slope is the AL_s value for the heel angle and speed for that series of tank tests. These tests and calculations must then also be carried out across the varying speeds and heel angles.

4.3.2 Inputs

Testing the Farr 52' model with no leeway or heel angle provides a baseline upright resistance model where the drag is sole a function of the velocity of the vessel. This data, appropriately scaled to the full sized ship, is displayed in Figure 10 below. As expected, the data points form a smooth curve increasing slowly at first but then rapidly as the speed of the vessel (in terms of its Froude number) grows.

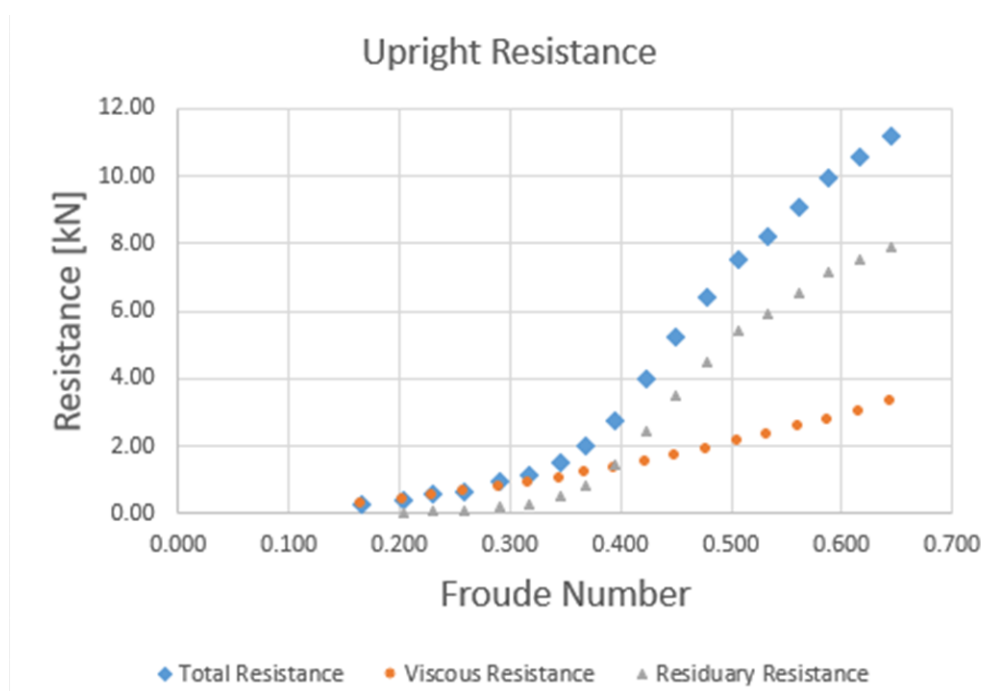


Figure 10: Upright resistance curve from experimental data

In the low speed regime, when Froude numbers are less than 0.35, the of the resistance of the ship increases slowly with speed as the total resistance is dominated by the viscous resistance component while the residuary component is negligible. Due to the fine hull lines oncoming water is able to gently flow past the hullform without much disturbance resulting in minimal wave-making. Further, the lack of heel or leeway means that there is no induced drag component. However, as the wave-making resistance grows much quicker than the viscous, at Froude numbers greater than 0.4 it becomes the dominant

resistance component. Around $F_n = 0.45$ the growth of the residuary resistance slows from nearly exponential to linear, and then, reaching an inflection point, slows down even further around a Froude number of 0.5. This series of upright resistance tests not only provided the requisite resistance curve for WinDesign VPP, but also validated tank testing procedures and data acquisition. Prior to this set of experiments the tow tank at the Solent University Hydrodynamics Centre had undergone various repairs and upgrades; thus, while the sensors had all been calibrated prior to being installed on the carriage, these resistance tests served to validate the control systems, software, and data processing systems and lend credibility to further, more complex tests to come.

As previously discussed, the R_0 , R_1 , and R_2 input values were calculated as the change in total resistance of the yacht with respect to the side force squared for a given heel angle and leeway.

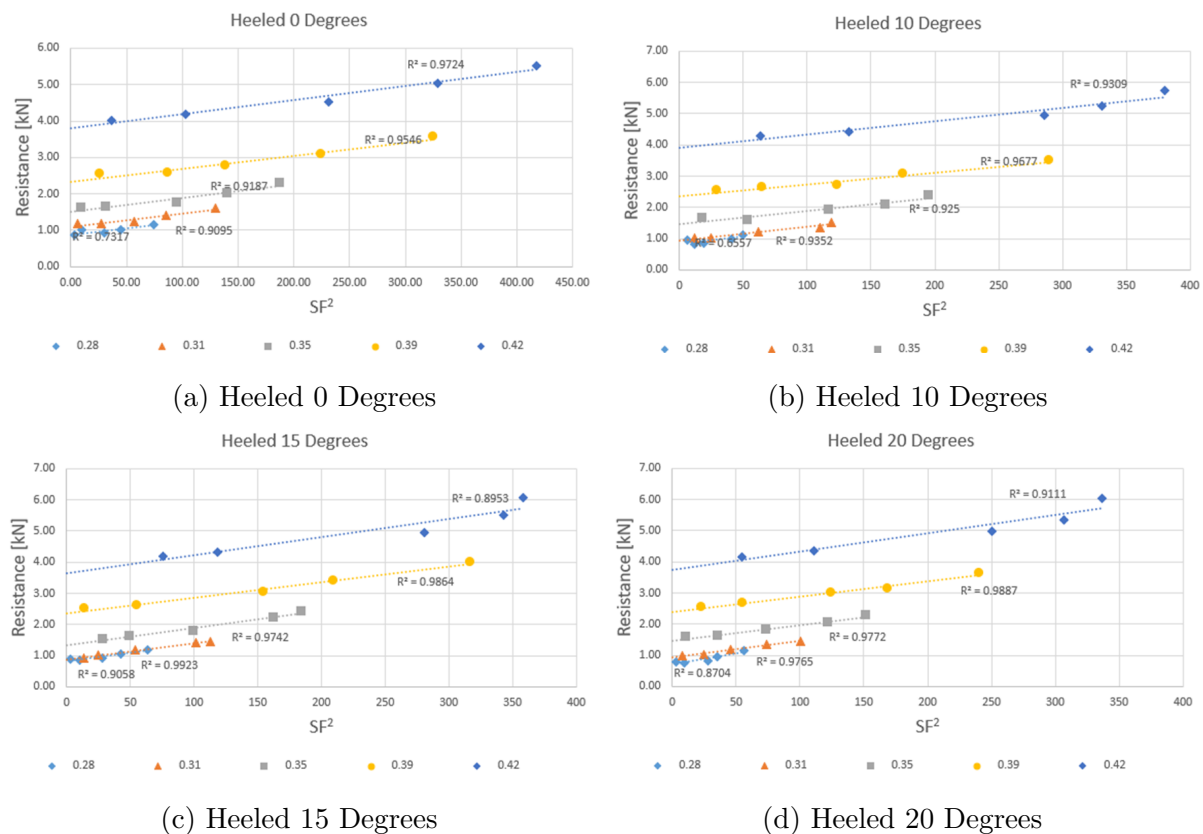


Figure 11: Resistance versus side force squared

By plotting different test series together, such as in Figures 11 and 12, different patterns

become more obvious. The first observation is that nearly every individual data set can be well modeled by linear regression lines with r^2 values nearly always greater than 0.9 (with the exceptions being the slow speed runs where any errors are intrinsically magnified). Next, the slopes of the regression fits are nearly all parallel which implies that heel angle and Froude number have little impact on the change in resistance with respect to leeway. Thus, while a yacht sailing faster will experience more resistance, the increase in resistance as a function of leeway will remain relatively constant regardless of speed (or heel angle).

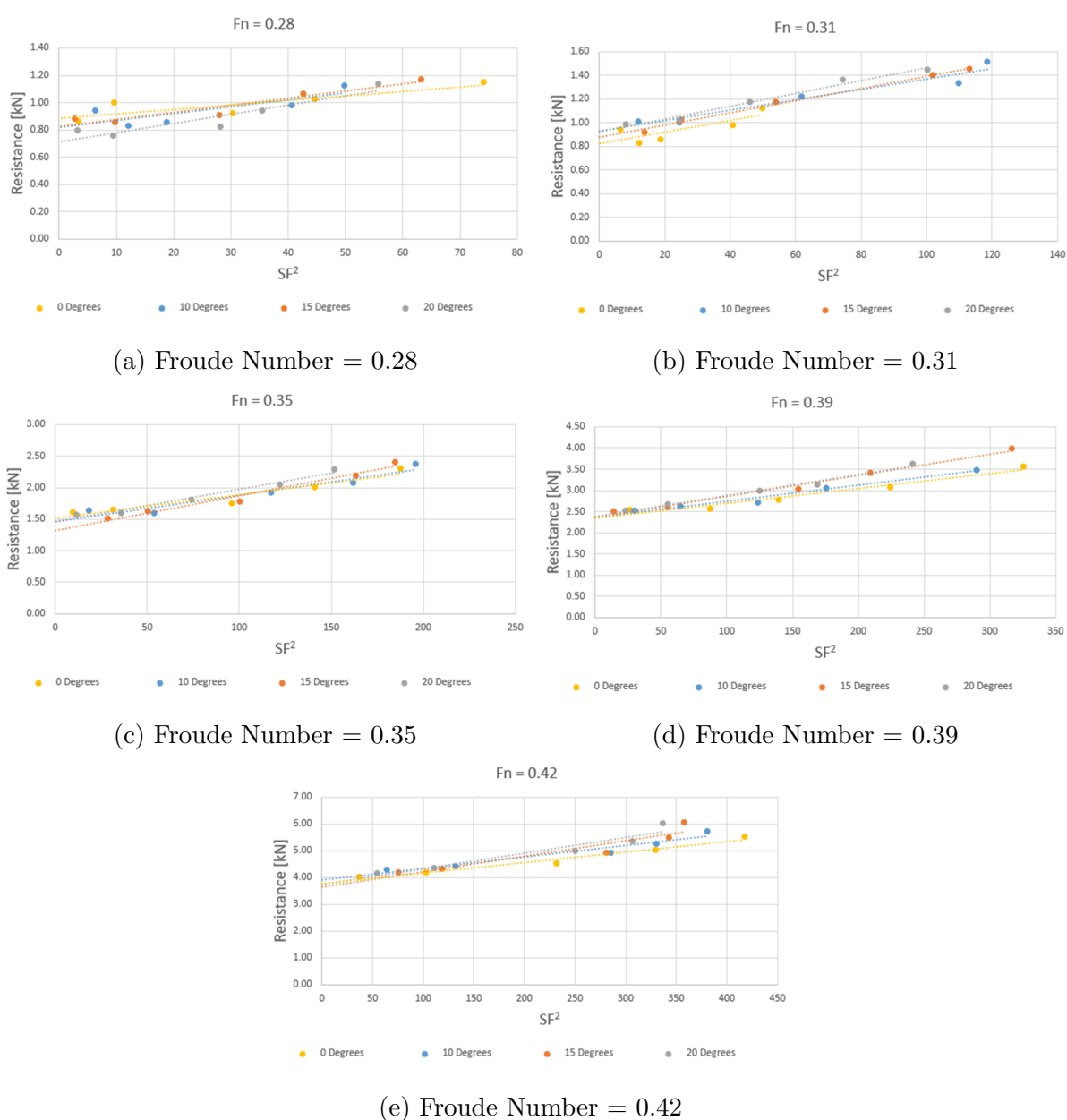


Figure 12: Resistance versus side force squared by Froude number

Extrapolating the plotted trend lines to the y-axis results in the R_0 values which the WinDesign VPP requires. The R_1 and R_2 values for each data set can be calculated by choosing two arbitrary side force values and determining the resulting resistance. Since the trend lines are linear, the actual side force values chosen have little impact though the WinDesign VPP program recommends representative values, thus side force squared values of 150 kN^2 and 300 kN^2 were chosen.

Similarly, plotting the side force (normalized by dynamic pressure) versus leeway angle yields the lift curve area plot from which AL_0 and AL_s can be obtained. As AL_0 is the lift that the yacht produces at zero leeway this value should be approximately zero which can be seen in the various subplots of Figure 13. The minor discrepancies observed can be attributed to slight imprecision in the leeway adjustment mechanism on board the carriage; unlike the heel fitting, the leeway fitting is not designed to lock in place at a specific angle but rather allows for continuous positioning across a range of values. This design increases the flexibility in leeway angle choices but decreases the reproducibility of a given angle and renders the precision of the angle measurements to only half a degree. Nonetheless, regression fitting minimizes these errors by averaging values across the five different leeway angles, resulting in AL_0 values with small deviations from 0.

4.3.3 Comparison

With the Farr 52' hullform and sail sets modeled and the direct experimental data input into WinDesign VPP the program calculates the expected boat speed across a range of wind speeds and angles. The resulting polar diagram, Figure 14, illustrates the optimized best speed for each wind speed and angle combination. In this diagram radial arcs represent boat speed, angles are true wind direction, and the plotted lines are the true wind speeds.

While VPP polar diagrams are incredibly useful for sailors as they graphically mimic sailing conditions and resulting boat speeds, they are less intuitive for comparison especially with respect to interpolation of data. Therefore, the results from the WinDesign VPP have been re-plotted on a Cartesian grid, Figure 15, where the x's indicate the transition

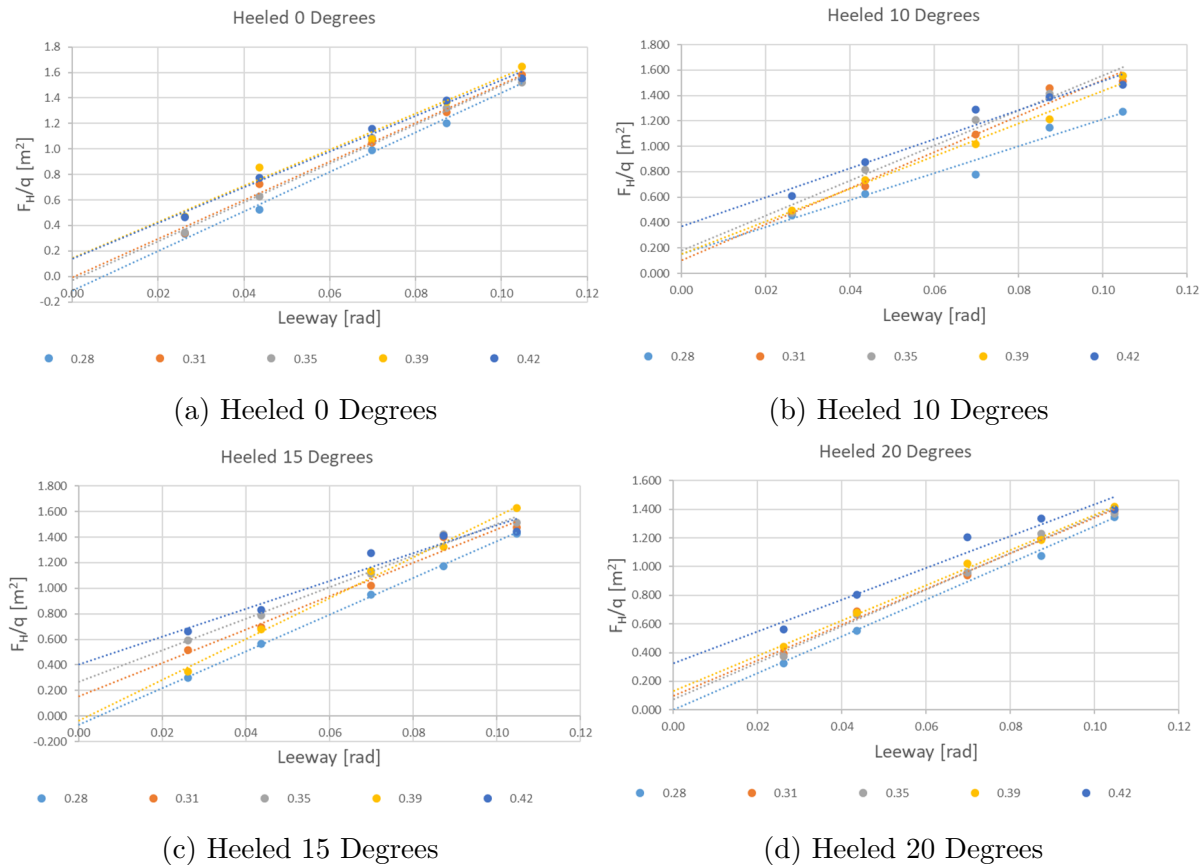


Figure 13: Side force versus leeway angle

from upwind to down wind sailing configurations. In this representation there is a clear increase in boat speeds as the wind angle increases with the effect being more noticeable in stronger wind conditions. For the weaker wind conditions this growth in speed dies off quicker and the boat speed curves plateau sooner than for the stronger winds.

The VPP developed thus far likewise displays velocity results in the standard polar diagram format, as seen in Figure 8, but for comparison's sake the results have been plotted in Cartesian coordinates. Running this VPP with the same hull and sail plan inputs then yields the predicted boat speeds which should be similar to those from the WinDesign VPP. The two velocity estimates are plotted in Figure 16.

Comparing the two VPP models there are clear similarities as well as distinct differences. To begin, they both exhibit reasonably smooth curves that are tightly grouped as one would expect considering that incremental changes in wind speed and direction should not result in dramatic changes in boat speed. Further, they both exhibit plateauing be-

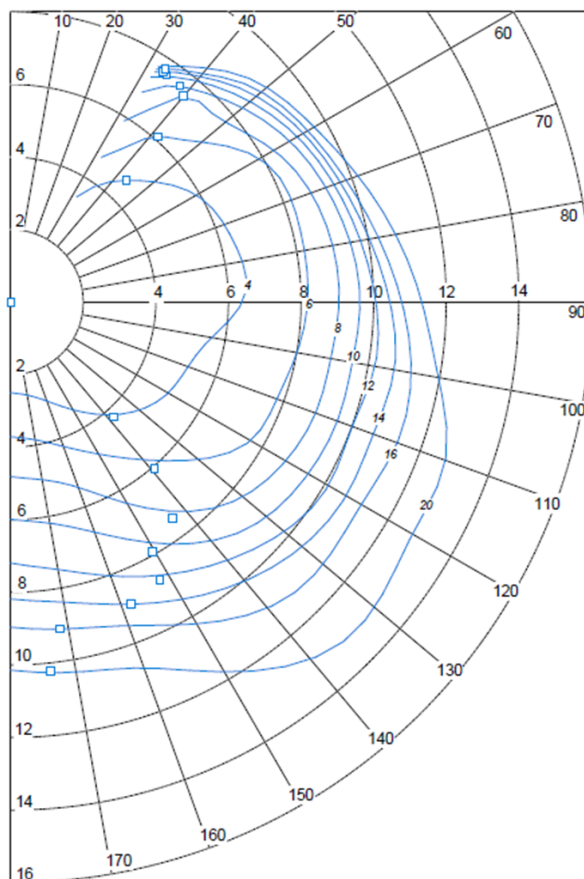


Figure 14: WinDesign VPP polar diagram

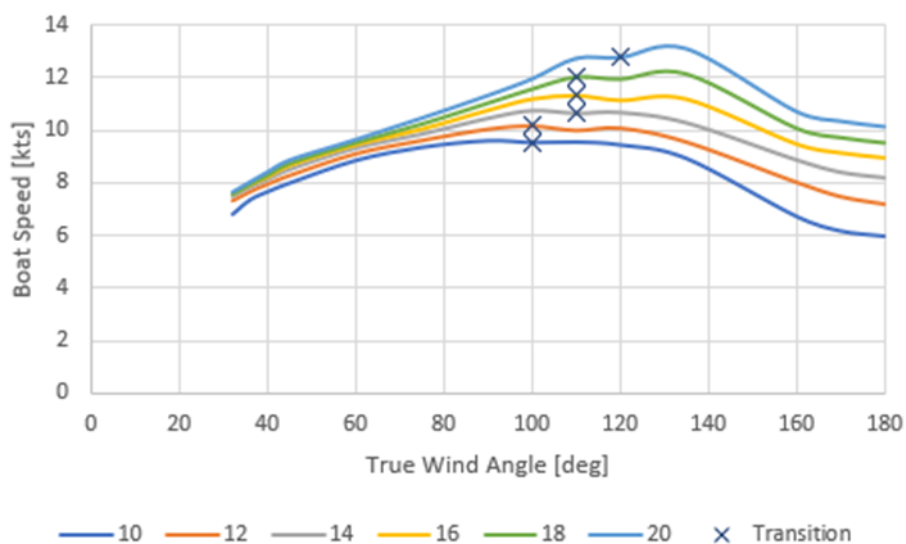


Figure 15: WinDesign VPP Cartesian diagram

havior when subjected to beam wind conditions (winds in the vicinity of 90 degrees). That is, however, where the differences begin to emerge with the WinDesign VPP plateauing at higher wind angles than the program developed in this section. The results from WinDe-

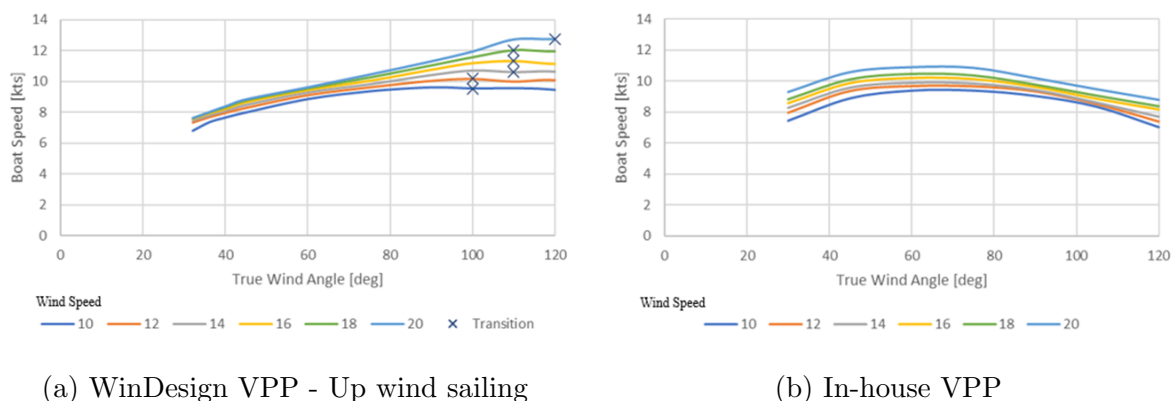


Figure 16: Comparison of boat speeds between two VPPs

sign VPP also depict a tighter grouping of boat speeds with respect to wind speed at small angles and a subsequent spreading out of the boat speed curves as the higher wind speeds induce plateauing behavior at higher wind angles. In the VPP developed, on the other hand, there is little change in the difference between the predicted boat speeds for different wind conditions with respect to true wind angles. Much of these differences can be attributed for in the way that the two different VPPs calculate the sail forces.

WinDesign VPP calculates sail forces through a programming loop that optimizes both *Reef* and *Flat* functions, thus providing estimated boat speeds based off optimally sized and shaped sails. On the other hand, the VPP developed in this paper enables the user to input the desired *Reef* and *Flat* values for each wind condition. This flexibility in allowing the user to tailor the program to how they would sail the yacht means that they results may not be the most optimal possible for the vessel (but rather for the sailor). Substituting the default *Reef* and *Flat* values (detail in Appendix 8.2.4) for those from WinDesign VPP results in the boat speed plot in Figure 17.

Using the updated *Reef* and *Flat* values it can be seen that the results now better match those from the WinDesign VPP with a much tighter grouping of boat speeds at smaller wind angles and a delay in the decrease in boat speed. However, these values also display more erratic behavior with respect to heel leeway angles than with the previous *Reef* and *Flat* values, which while similar to WinDesign VPP appear questionable.

Figure 18 illustrates the heel angles that WinDesign VPP calculates for each wind condi-

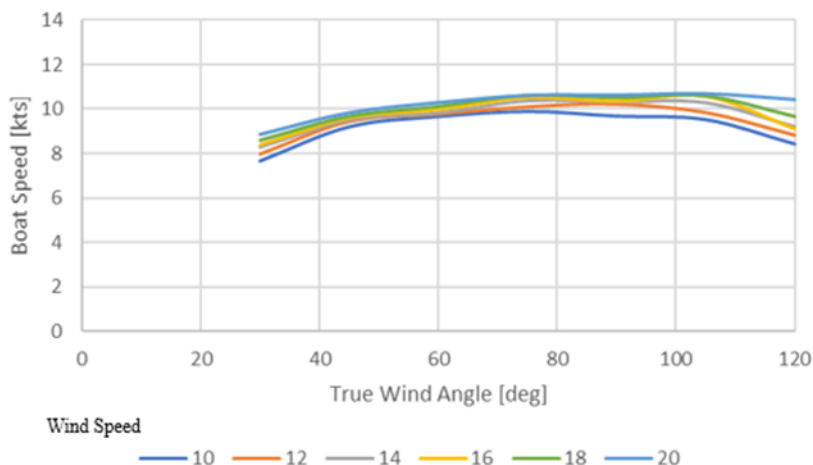


Figure 17: VPP Cartesian diagram with WinDesign *Reef* and *Flat* values

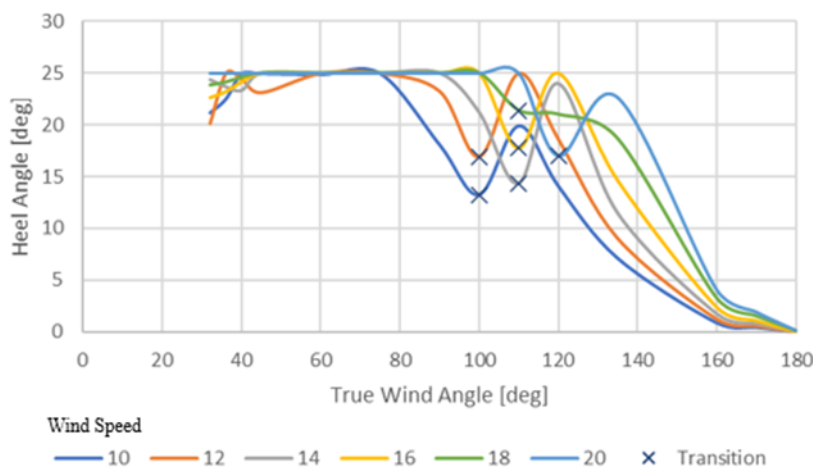
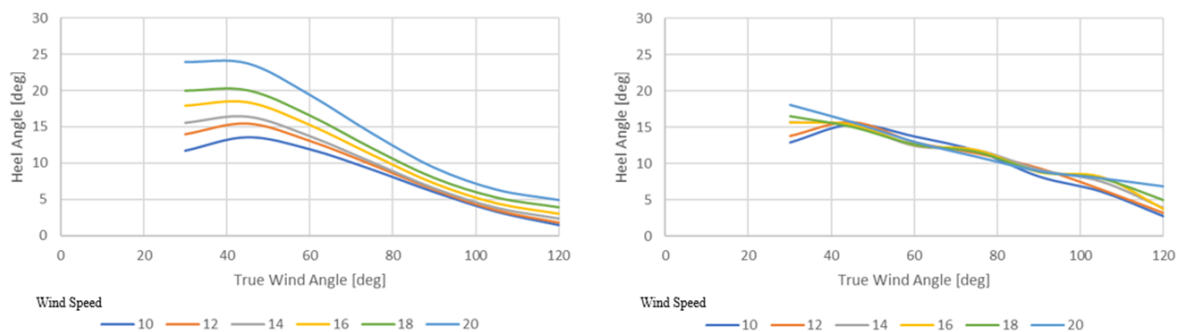


Figure 18: WinDesign VPP calculated heel angles

tion. Unlike the speed plots, this one is much more erratic with counter-intuitive dips and a penchant for high angles. Interestingly, significant dips coincide with each transition from upwind to downwind conditions which are likely artifacts from the optimization programming but illustrate how mathematically optimal solutions are not always reasonable in the physical world. The developed VPP with default *Reef* and *Flat* values, on the other hand, exhibits smooth curves that behave as an experienced sailor would expect them to as illustrates in sub-figure 19a. When WinDesign's *Reef* and *Flat* values are introduced, much of the nature of the curves remains but they do become more lumpy and produce questionable results.

It should be noted, however, that in general VPPs are designed towards precision and not



(a) VPP heel angles with default *Reef* and (b) VPP heel angles with WinDesign *Reef* and *Flat* values

Figure 19: Comparison of the effect of *Reef* and *Flat* values on heel angles

necessarily accuracy; that is, they are much better at predicting boat speed trends than actual speeds. So, while for the same inputs WinDesign VPP and the VPP developed thus far do not perfectly agree, they are sufficiently close and both present reasonably sound results.

5 ADDITION OF FOILS

The first recorded patent for hydrofoils on a watercraft was issued in 1869 for the installation of a series of inclined planes or wedges along the length of a ship designed to reduce the vessel's draft as it is driven forwards. Shortly before the turn of the twentieth century this idea was modified by rearranging the foils into a vertical array. This ladder system had the benefit of reducing foil area as the hull lifted out of the water, reducing resistance. As the understanding of the physics of foils and lift modeling increased in the early twentieth century so to did enthusiasm around hydrofoils with the adoption of the concept to high speed vessels, particularly by various navies around the world. By the 1950's hydrofoils had been pushed to their physical limits as cavitation prevented further increases in speed until the development of supercavitating foils. However, by this time, enthusiasm had begun to wane with designers generally favoring efficiency over speed.

Due to their decreased and more variable speed ranges, sailboat designers did not adopt hydrofoils for nearly a hundred years after their invention. In 1983 the sailing world was forever changed by the 12 meter Australia II outfitted with a winged keel. In part due to the increased maneuverability and additional righting moment provided by the wing shaped foils attached to the keel the Australia II won the America's Cup. Though not explicitly forbidden controversy over the design undoubtedly led to a distaste for hydrofoils in the sailing world. Thirty years later, the 2013 edition of the America's Cup explicitly allowed hydrofoils and the sight of 22 meter catamarans flying across San Francisco harbor on foils captivated the world and ushered in a new era in sailing. Since then, foils have been adopted across a variety of classes of sailboats and have become an integral part of racing competitions. Earlier in 2023, Baltic Yachts unveiled the Baltic 111 Raven, a 34 meter foiling super-yacht, the debut of foil assisted sailing in the luxury yachting world, signalling a potential shift in cruising yachts.

5.1 Theory of Foiling

Foils, being underwater appendages which generate lifting forces, can provide two different benefits to a sailing vessel depending on their shape and orientation. Shallow, horizontal

foils generate a vertical lifting force which lifts the hull out of the water, decreasing the underwater volume and wetted surface area and thus reducing both residuary and viscous resistance components. Deep, vertically oriented foils are capable of generating horizontal forces which counteract heeling due to wind loading of the sail set. The additional righting moment provided by the hydrofoils allows a yacht to sail more upright, presenting a larger sail area to the oncoming wind and enabling faster speeds. Modern sailboats typically have foils that are a hybrid: plunging vertically into the water before curving horizontally so as to minimize foil ventilation and surface effects while optimizing the lift generation at specific heel angles.

Care must be taken in the design and implementation of foils as an improperly balanced hull-foil system can lead to negative outcomes in two main ways due to the magnitude and direction of lift generated. First, if insufficient lift is generated to significantly raise the hull out of the water or decrease heel angle, the reduction in speed due to the resistance of the lifting surfaces will be greater than their intended speed gains resulting in an overall reduction in speed. Second, improperly balanced force couples generated by foils can also have adverse effects. For example, a foil designed to lift a hull out of the water that is not positioned properly can create a heeling moment due to horizontally eccentric loading; similarly, a foil that is intended to provide additional righting moment can create a negative side force, causing the boat to crab, inducing greater resistance and negating expected benefits. In addition to the already complex interaction of forces in three degree of freedom VPP, the existence of foils further complicate the matter, rendering it nearly impossible to determine the efficacy of hydrofoils without detailed, in depth calculations even for the most simple of foil forms.

Lifting line theory provides a simple yet sufficiently accurate method of calculating the lift generated by a foil. The complex geometries of modern foils can be decomposed into smaller, straight segments which approximate the original shape and lift generation. For explanation purposes, only one segment will be taken into account but in reality multiple segments may have different dimensions and orientations. As with the sails, a hydrofoil generates lift perpendicular to its span and drag parallel to its velocity (though in opposite direction). Thus, as with the sail set, the lift generated by a foil can be expressed as:

$$L = \frac{1}{2}\rho V_f^2 A_{Plan} C_{L,3D}$$

where V_f is the velocity of foil, A_{Plan} is the planform area of the foil, and $C_{L,3D}$ is the 3D coefficient of lift of the foil. In much the same way that the angle of attack of a sail affects its apparent wind speed, so too does the angle of attack of an underwater foil affect the effective encounter speed of water. Assuming there is no current, the the flow of water past the foil is proportional to the speed of the yacht and can be determined by the equation below where α is the static angle of heel of the foil.

$$V_f = V_b \sqrt{(\sin \beta \sin (\phi + \alpha))^2 + (\cos \beta)^2}$$

In lifting line theory, the coefficient of lift of a three dimensional wing, $C_{L,3D}$, can be calculated from the two dimensional lift coefficient and the effective aspect ratio, AR_e , of the wing. The formulation for the 3D coefficient proposed below takes into account the loss of lift due to tip vortices which decrease as a percentage of total lift as the aspect ratio increases.

$$C_{L,3D} = \frac{C_{L,2D}}{1 + \frac{3}{AR_e}}$$

Similarly, the drag acting on a foil can be described in terms of its dynamic pressure, planform area, and 3D coefficient of lift, $C_{L,3d}$.

$$R_{D,3D} = \frac{1}{2}\rho V_f^2 A_{Plan} C_{D,3D}$$

For the drag, however, the coefficient of drag of the 3D foil is a sum of the 2D coefficient of drag, $C_{D,2D}$, and the induced drag, $C_{D,I}$. Since the induced drag is a function of the lift of foil and the apparent speed of the foil, $C_{D,3D}$ can be calculated as:

$$C_{D,3D} = C_{D,2D} + C_{D,I} \quad \text{where} \quad C_{D,I} = \frac{C_{L,3D}^2}{\pi AR_e}$$

The 2D coefficients of lift and drag are dependent on speed, angle of attack, and foil profile shape. For the foil geometry, an Eppler E-817 profile was chosen as it provides good lift to drag ratios for the Reynolds numbers that hydrofoils typically operate at and is less susceptible to cavitation than other common foil shapes (such as various NACA families of profiles). Using XFOIL, a program designed for the analysis of subsonic foils,

the coefficients of lift and drag for this foil shape were then calculate across a range of angles of attack and Reynolds numbers sufficient to cover the scope of operation of a hydrofoil; that is, angles of attack from -2 to 10 degrees and Reynolds numbers from 4×10^5 to 5.2×10^6 (Reynolds numbers which, for a foil with a chord of 0.7 m, equate to a speed range of $0.66 \frac{m}{s}$ to $8.62 \frac{m}{s}$ or 1.3 to 16.8 knots). XFOIL is a high-order, panel method solver capable of viscous analysis initially designed for airfoils (Drela and Youngren 2001), however, since it bases calculations off the Reynolds number and makes no assumptions on fluid density (or other medium properties) the program can be used for foils operating in other fluids, a practice the program's author, professor Mark Drela of MIT, agrees with (Drela, personal communication). However, at the lower end of this range of Reynolds numbers the program (below 1.5×10^6) the program is less numerically stable, particularly at high angles of attack (above 8 degrees), though these numerical instabilities are of minimal consequence since foils operating at such speeds generate little lift compared to the forces acting on the rest of a ship.

The calculated coefficients of lift and drag were then tabulated into respective tables. These two data sets could then be used as $C_{L,2D}$ or $C_{D,2D}$ look up tables for any of the discreet Reynolds numbers and angle of attack values calculated. In order to expand the capabilities beyond these discrete values a bilinear interpolation function was written which is explained in further detail in Appendix 8.7.4.

While the range of angles of attack does seem excessively broad (ranging from -2 to 10 degrees), this scope is warranted given that the apparent angle of attack of the foil, ξ , is affected not only by the static angle of the foil but also the heel and leeway of the yacht it is attached to. The equation below describes these relationships with the 180° included to reconcile sign conventions; this equation (and subsequent ones in this section) is derived in Appendix 8.6 and are based off the work of Gournay 2022.

$$\xi = \tan^{-1} (\tan \beta \sin (\phi + \alpha + 180^\circ))$$

This apparent angle of attack is then used not only for the determination of $C_{L,2D}$ and $C_{D,2D}$, since it is the angle at which the foil is moving through the water, but also for rotating the forces developed by the foil from the foil frame of reference to that of the

sailboat. With respect to its own frame of reference the foil generates both lift and drag, however, to the ship as a whole these forces can be resolved as a vertical lift, a lateral side force, and drag opposite to the vessel's velocity. The vertical lift force, taking into account α , ϕ , and ξ is:

$$L = (L \cos \xi - R_{D,3D} \sin \xi) (\cos (\phi + \alpha))$$

Likewise, the side force generated by the foil can also be calculated as a function of the lift and drag with respect to the heel of the yacht as well as the static and apparent angles of attack of the foil.

$$SF = (L \cos \xi - R_{D,3D} \sin \xi) (-\sin (\phi + \alpha))$$

The drag developed by the foil which counters the vessel's velocity can be calculated in a similar manner, however, to account for the leeway of the vessel a modification value, η , must be taken into account.

$$D = (R_{D,3D} \cos \xi + L \sin \xi) (\cos (\beta - \eta))$$

$$\eta = \tan^{-1} (\tan \beta \sin^2 (\phi + \alpha))$$

With the lift and side force generated by the foil calculated in the global frame of reference of the entire vessel, these effects can then be resolved into the resultant righting moment of the ship due to the foil. As a moment is simply a force applied at a distance, the righting moment is the combination of the lift and side forces multiplied by their eccentricity where CoE_y is the lateral distance from the center of effort of the foil to the centerline and CoE_z is the vertical distance from the center of effort to the waterline.

$$RM_{Foil} = L \times CoE_y \cos \phi - SF \times CoE_z \cos \phi$$

Thus far, the developed VPP has three degrees of freedom: velocity, heel, and leeway - each associated with one of the balanced force couples: drive force and resistance, righting moment and heeling moment, and keel and sail side forces. If attached foils produce significant vertical lift, a fourth degree of freedom is required to properly model the ship's behavior. As a ship raises out of the water, not only does its draft decrease but due to the

underwater geometry of its hull so to do the beam, and waterline length change (as well as the displacement and all related parameters). However, despite the complex curvature of the hull many of the ship's hydrostatic parameters vary nearly linearly with changes in displacement as hydrostatic curves calculated by Maxsurf in Figure 20 illustrates for the Farr 52' model.

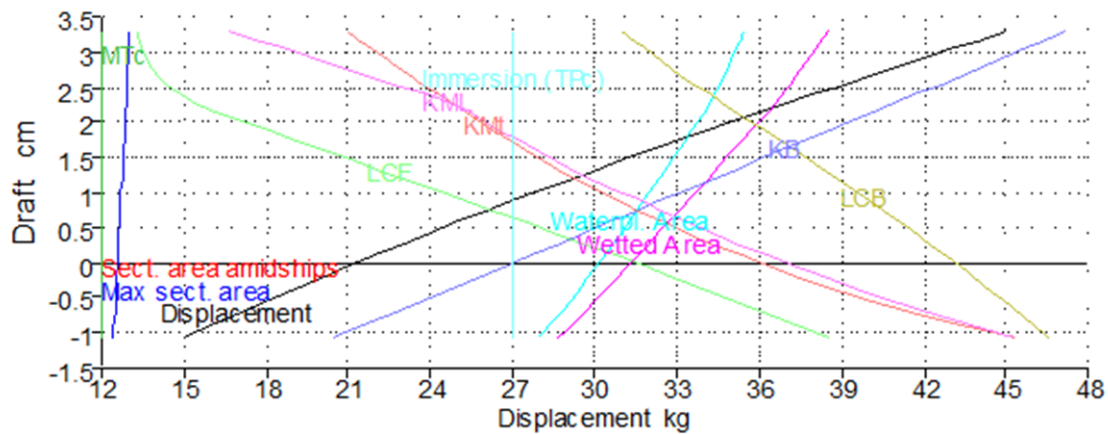


Figure 20: Farr 52' model hydrostatic curves of form

By multiplying the change in displacement by a linear approximation of the slopes of the hydrostatic curves of form the changes in the ship's hydrostatic parameters due to the hull lifting out of water can be reasonably well estimated. Therefore, the VPP is able to take into account the effects of vertical lift by first converting the lifting force into an equivalent reduction of displacement (by converting the lifting force in Newtons to metric tonnes) and subtracting that difference from the original displacement of the ship, Δ_0 , to find the new displacement, Δ_{new} . Then for any parameter, X , the new value modified by the lifting force can be determined as:

$$X_{new} = \left(1 - \left(1 - \frac{\Delta_{new}}{\Delta_0} \right) \frac{\partial X}{\partial \Delta} \right) X_0$$

where $\frac{\partial X}{\partial \Delta}$ is approximated by the linear change in the parameter with respect to the change in displacement of the sailboat. If for each wind condition the original hull parameters are replaced by these new approximations then as the VPP iterates to find a solution to the optimization problem it also implicitly takes into account the effects of vertical lift generated by the foils. Though the macro only solves three optimization problems, in effect it balances forces along four degrees of freedom: surge, roll, pitch and now also heave.

5.2 Experimental Investigation to Determine Foil Aspect Ratio

As previously discussed, the lift generated by hydrofoils, and thus their impact on boat performance, is affected by their shape and the speed of water flowing past them. The speed component is relatively straight forward as it is a function of the speed of the yacht and the foil's three dimensional angle of attack. The shape of the foil, on the other hand, is much more difficult to take into account. For a two dimensional foil, the coefficient of lift is a function of the profile shape and angle of attack which can easily be referenced for most common foils. For an infinitely long, prismatic foil (that is, one where the cross section does not change across the span) the flow around the foil is identical to the two dimensional case. However, real world foils do not have infinite aspect ratios; instead, they have a finite length and typically at least one free end. At these free wing tips, the difference in pressure above and below the foil induce tip vortices, decreasing the difference in pressures and ultimately decreasing the lift generated. These tip vortices have the effect of decreasing the pressure difference across the span of the wing with minimal influence at the root (where there is often a mirror effect) to the wing tip where there is no pressure difference between above and below the foil. Lifting line theory takes tip vortices into account by using an effective aspect ratio, AR_e , which is the geometric aspect ratio reduced by a factor relative to the spanwise shape of the foil. Likewise, the position of the center of effort of the foil is affected by tip vortices. Since the the root end of a wing is contributing far more to the lift generation than the tip end, the spanwise position of the center of effort shifts closer to the root.

Thus, in order to take into account the lift generated by foils, their effective aspect ratio and center of effort must be known. Tow tank testing was conducted to create a mathematical model detailing the effect of leeway angle, speed, and geometric aspect ratio on the position of the center of effort and effective aspect ratio of a submerged foil. To do so, Solent University Hydrodynamics Centre's IMOCA Open 60 model was used as it has a hullform comparable to the Farr 52' and Delft series hulls and already had slots for adjustable daggerboards. Vertically oriented, daggerboards are typically installed in sailing vessels to provide additional side force; thus, while they are positioned much differently from typical hydrofoils, the water flow around them is comparable and thus the results should be analogous.

The model was first tested without a daggerboard installed (alternatively, an aspect ratio of 0) at five different Froude numbers to determine the bare hull resistance and act as a calibration test to zero future results. Next the model was tested at the same speeds while outfitted with daggerboards with geometric aspect ratios of 3, 4, and 5. Finally, the previous tests were conducted but at leeway angles of 2 and 3 degrees.

Subtracting the bare hull side force determined during the first set of runs (which arose from any slight asymmetries and imperfections in the hull) and dividing by the cosine of the daggerboard's angle of inclination yielded the lift generated perpendicular to the foil itself. Plotting the lift generated during each tow tank run provides a good qualitative overview of the effects of aspect ratio and leeway angle (as can be seen in Figure 21). For the first runs, without a daggerboard installed, there is minimal lift generated as expected since there is no foil to produce lateral lift. For the next set of runs, when the daggerboard has an aspect ratio of 3, increasing the speed of the vessel increases the lift generated following a quadratic growth pattern. Increasing the aspect ratio of the foil further increases the lift generated, particularly at higher speeds, as there is more surface area to generate lift. It can also be observed that as the leeway angle of the vessel increases from 0 to 2 degrees and then 3 degrees, the lift also increases with gains once again being more prominent at high speeds. Of note, on the model used, the daggerboard fitting was permanently set to an angle of attack of 4.4 degrees, thus, the true angles of attack of the different test runs were 4.4 degrees, 6.4 degrees, and 7.4 degrees which explains the large amounts of lift generated at a leeway angle of zero degrees, and the comparatively small increases thereafter.

With the lift generated from each run measured, the respective three dimensional coefficients of lift for each tow tank test run can be calculated as:

$$C_{L,3D} = \frac{L}{\frac{1}{2}\rho V^2 A} \quad \longrightarrow \quad \frac{L}{\frac{1}{2}\rho V^2 \text{chord} \times \text{span} \times e}$$

where, according to lifting line theory, the lifting area, A , can be calculated as the product of the chord and span multiplied by an efficiency factor, e , which takes into account the decrease in lift due to tip vortices. Further, since the two dimensional lift coefficient for

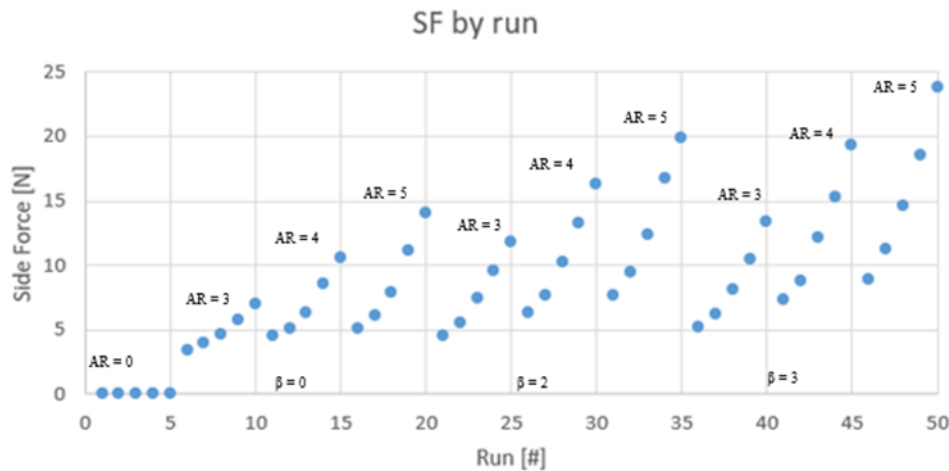


Figure 21: Lift generated perpendicular to daggerboard

the daggerboard foil profile can be approximated as $0.11 \times \alpha$, then, using the following identity the expected three dimensional lift coefficient can be calculated based on the effective aspect ratio, AR_e .

$$C_{L,3D} = \frac{C_{L,2d}}{1 + \frac{3}{AR_e}} \quad \longrightarrow \quad AR_e = \frac{3}{\frac{C_{L,2D}}{C_{L,3D}} - 1}$$

Calculating the effective aspect ratios across the range of speeds and leeway angles tested yielded the result that on average the effective aspect ratio, including mirror effects, was 110% of the geometric aspect ratio (without mirror effects). While counter intuitive that the effective aspect ratio should be larger than the geometric one, the hull at the root end of the daggerboard acts as a flat plate capping the foil creating a strong mirror effect and increasing the effective aspect ratio of the foil as a whole.

The spanwise center of effort was similarly determined for each daggerboard test run by dividing the measured heeling moment caused by the daggerboard by the measured side force. The resulting distances were with respect to the heel fitting attachment on the model. Subtracting the distance from the center of rotation of the heel fitting to the root of the foil from the previously calculated distances provided the location of the center of effort on daggerboard for each run. Using this procedure it was found that, on average, the location of the center of effort was only one quarter span of the foil. While this value seems lower than one would expect, considering that the effective span of the foil is only 55% of the actual span this value becomes much more reasonable. It should be

understood, however, that while proper tank testing procedures were followed, the measurements required to determine the effective aspect ratios and centers of effort involved measurements in millimeters on a model over 2 meters in length. Thus, even the slightest mismeasurement results in compounding errors which are magnified through calculations (in particular division).

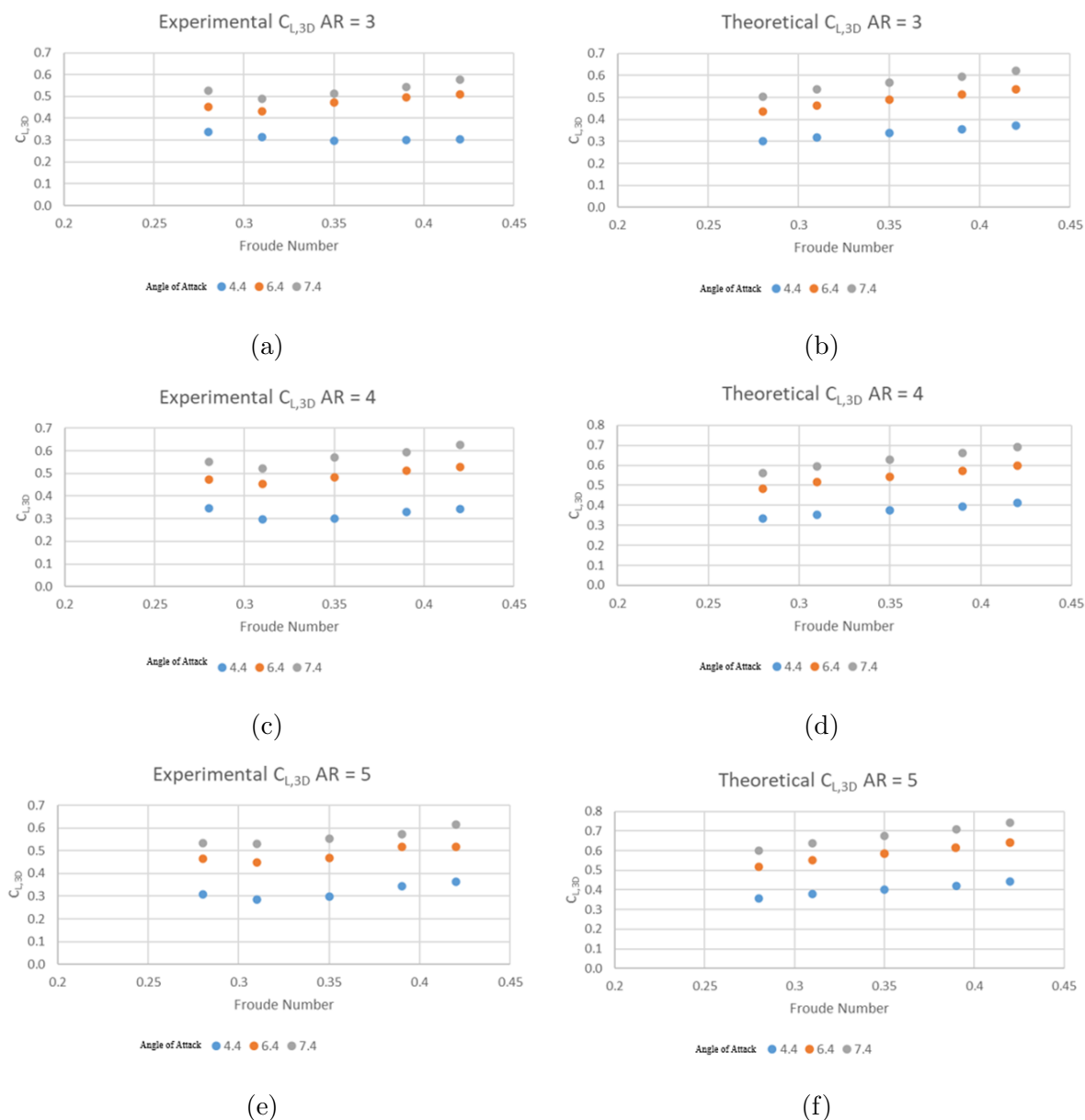


Figure 22

6 EFFECT OF FOILS ON SAILING PERFORMANCE

6.1 Farr 52'

With the VPP modified to take into account the lifting and righting effects of foils it then must be tested, a procedure which will validate the implementation of the foils and provide a greater understanding of the effect of the foils on the original sailing yacht. While the Farr 52' is not a yacht that would typically be outfitted with hydrofoils, it is a well studied hullform which has been extensively used in validation of this VPP due to its similarity to Delft series hulls. Hence, this hullform ought to provide an adequate platform for evaluating the effectiveness of the attached foils. For simplicity's sake a 2.1 meter foil with a chord of 0.7 meters and thickness of 0.07 meters comprised of a single section with an Eppler 817 profile is used in conjunction with the Farr 52' hull. The foil is rotated 20 degrees from horizontal (to ensure sufficient underwater submergence) and has an angle of attack of 1 degree (so that the effective angles of attack remain within the tabulated data set). While basic in form, this foil's effects are significant enough to provide representative results. Running the VPP with the foil attached at the same wind speeds and heel angles allows for a comparison between the bare hull (with keel but without foil) and with the foil attached, thus allowing for an analysis of the effects of the foil as can be seen in Figure 23.

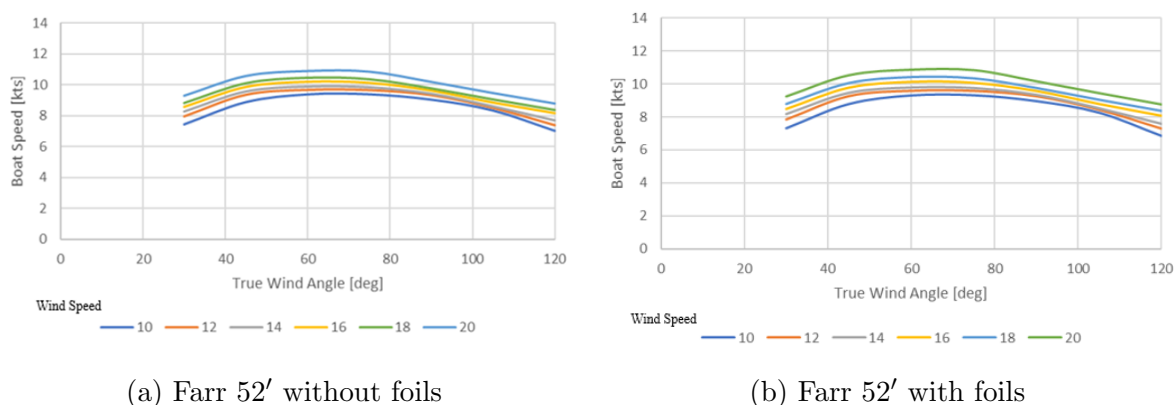


Figure 23: Comparison of boat speeds with and without foils

Interestingly, subfigures 23a and 23b appear nearly identical, which, at first glance seem to imply that the foils are ineffective. However, considering that the submerged foil is contributing to the overall viscous resistance of the hull and inducing additional drag the foil must be providing sufficient lift to counter its additional resistance. This is done in

two way, through vertical lift and righting moment. Because the foil is oriented at a reasonably shallow angle it is able to create a vertical lifting force to raise the hull out of the water and decrease the wetted surface area of the hull, thereby decreasing the resistance of the hull; however, the Farr 52' is an older style race-cruising yacht which is considerably heavier than those in use today and due to its large displacement the vertical lifting force generated by the foil is negligible (in this case at least). The righting moment generated by the foil, however, is significant compared to the heeling moment of the ship and this enables the ship to sail more upright, increasing the sail area exposed to the wind, and creating a large enough drive force to counter the added resistance of the foil. Of note, as the heel angle decreases, the wetted surface area of the Farr 52' actually increases (see Figure 3) and thus any additional drive force resulting from sailing more upright must also overcome the added viscous resistance of sailing more upright. The reduction in heel, when plotted against true wind angle and wind speed is illustrated in Figure 24.

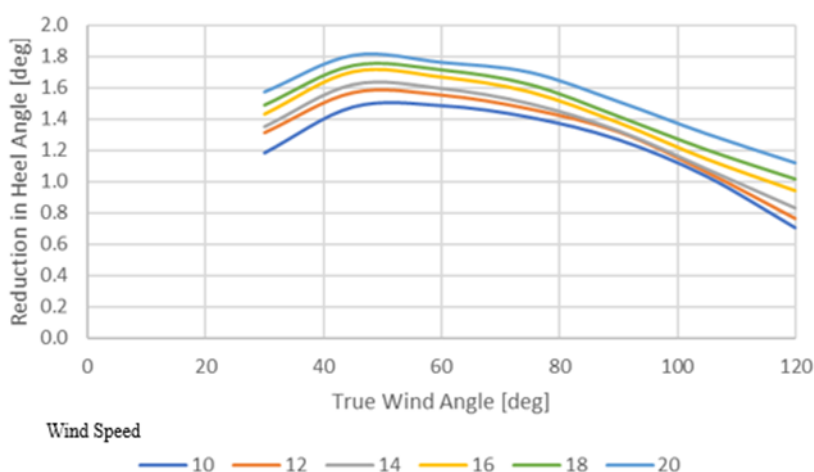


Figure 24: Reduction in heel angle due to foil

In general, as the speed of the boat increases, there is a commensurate increase in the additional righting moment generated by the foils and thus a near proportional decrease in the heel angle of the vessel. However, due to the non-linear nature of the system this increase in righting moment is greatest at small wind angles.

6.2 IMOCA Open 60

The lack of appreciable speed change observed with the addition of foils to the Farr 52' has less to do with the efficiency of the foils but rather the hullform of the vessel. Designed well before the adoption of foils to sailboats, the Farr 52' displaces too much water (compared to its length) to effectively be lifted out of the water and its reduction in wetted surface area with heel negates much of added benefit of the supplemental righting moment that foils provide. Thus, while the Farr 52' is a well designed boat it is poorly adapted to using foils; contemporary designers have noticed this phenomenon among older boats and instead are beginning to design hulls around the use of foils vice the other way around. Modern racing yachts, such as the IMOCA Open 60 class where the use of foils is prevalent, are significantly lighter than their predecessors with shallower deadrise angles to assist in planing. Using the same rudimentary foil as before but installed on a Lazare Open 60 yields the results tabulated in Figure 25 (principle characteristics for the Lazare Open 60 can be found in Table 7 in Appendix 8.3).

		True Wind Speed [kts]								True Wind Speed [kts]					
		10	12	14	16	18	20			10	12	14	16	18	20
True Wind Angle [deg]	30	7.25	7.88	8.31	8.85	9.30	9.95	True Wind Angle [deg]	30	-0.34	-0.16	-0.08	-0.07	-0.06	-0.05
	45	9.12	9.86	10.25	10.72	11.09	11.48		45	-0.07	-0.04	-0.03	-0.01	0.01	-0.01
	60	9.94	10.51	10.87	11.30	11.55	11.98		60	-0.04	0.00	0.01	0.01	0.02	0.04
	75	10.00	10.57	10.90	11.34	11.61	12.13		75	-0.03	0.01	0.03	0.03	0.05	0.09
	90	9.44	10.05	10.17	10.60	10.93	11.54		90	-0.05	0.00	0.01	0.04	0.07	0.07
	105	7.96	8.36	8.58	9.08	9.50	10.25		105	-0.14	-0.10	-0.09	-0.05	-0.02	0.02
	120	6.15	6.69	7.14	7.72	8.22	8.97		120	-0.17	-0.13	-0.11	-0.09	-0.07	-0.04

(a) Lazare Open 60 without foils

(b) Lazare Open 60 with foils ($AR = 2$)

Figure 25: Comparison of Lazare Open 60 boat speeds with and without foils

Subfigure 25a, on the left, is the true boat speed (in knots) of the Lazare Open 60 for the given wind speeds and angles calculated by the VPP and subfigure 25b is the difference in boat speed with the addition of foils where values highlighted in green indicate wind conditions where the boat with foils is faster than without and those highlighted in red indicate slower speeds. These tables illustrate the non-uniform effect the foils generate across wind speeds and directions due to the complex non-linear interactions between forces. The dominant trends that can be observed are a decrease in performance when sailing close to the wind and when the wind is abaft the beam as well as at low wind speeds and an increase in performance when sailing in high winds forward of the beam.

These trends are exaggerated as the aspect ratio of the foil increases, increasing the vertical lift and righting moment, as tabulated in Figure 26.

True Wind Angle [deg]	True Wind Speed [kts]						True Wind Angle [deg]	True Wind Speed [kts]					
	10	12	14	16	18	20		10	12	14	16	18	20
30	-0.66	-0.26	-0.16	-0.14	-0.11	-0.08	30	-1.05	-0.34	-0.25	-0.21	-0.17	-0.11
45	-0.13	-0.06	-0.04	0.00	0.01	0.00	45	-0.21	-0.09	-0.05	0.03	0.02	0.03
60	-0.07	0.01	0.05	0.04	0.07	0.11	60	-0.10	0.04	0.12	0.11	0.17	0.26
75	-0.04	0.06	0.10	0.10	0.15	0.23	75	-0.04	0.15	0.20	0.25	0.35	0.47
90	-0.09	0.03	0.04	0.12	0.16	0.21	90	-0.13	0.07	0.11	0.27	0.30	0.52
105	-0.28	-0.20	-0.16	-0.09	-0.03	0.06	105	-0.47	-0.35	-0.27	-0.15	-0.04	0.14
120	-0.33	-0.25	-0.22	-0.17	-0.14	-0.08	120	-1.42	-1.00	-0.49	-0.28	-0.23	-0.13

(a) Lazare Open 60 with foils ($AR = 3$)(b) Lazare Open 60 with foils ($AR = 4$)

Figure 26: Comparison of change in boat speeds due to AR

The aspect ratios of the foils were adjusted by modifying the span of the foils while maintaining all other parameters (such as chord, thickness, and angle of attack). Since the wetted surface area of the foil changed with these adjustments they had the effect of both increasing drag and increasing lifting forces. At low speeds there is insufficient flow over the foils to generate enough lift (and thus create righting moment and lift the hull out of the water) to counteract the additional resistance of the foil. However, when the yacht is sailing at higher speeds, the vertical lift and righting moment generated are even greater due to the enlarged lifting surface resulting a a drive force great enough to overcome the additional wetted surface resistance.

7 CONCLUSION

The complex interaction of forces that make prediction of sailboat performance difficult are exactly what make this VPP function. Reflecting on the first principles of engineering, in order for a system to be in dynamic equilibrium the sum of all the forces must be zero. For a sailing yacht with three degrees of freedom (and thus constrained in the other three degrees) this implies that the drive force must equal the resistance, the heeling moment must equal the righting moment, and the keel and sail side forces must be equal. The coupled nature of these forces complicates solving for dynamic equilibrium as all the equations need to be solved simultaneously but it also implies a confidence in a calculated solution due to the sensitivity of the system to small changes (for example the resistance cannot change without altering the heel and leeway angles so either they are all correct or all incorrect). The program is generalized to include a fourth degree of freedom by modifying the program to consider the effects of the change in displacement on the change in the other input parameters (such as length, beam, etc.). In doing so, hydrofoils can be explicitly considered as a combination of additional forces (lift, drag, and side force) and a first order approximation of their effects on the other forces the yacht experiences.

As a three degree of freedom VPP (constrained in heave, that is, without the addition of foils), this program demonstrates comparable results to commercially available VPPs. Using a Farr 52' hullform as a test platform, the developed VPP produced results with strong similarities to those determined by WinDesign VPP. Though there were differences in calculated boat speeds, the strength of a VPP are not its ability to perfectly identify the speed a yacht will sail at but rather predict overall trends with respect to wind conditions and sailboat parameters. One of the largest sources of discrepancy between the two VPPs was the determination of *Reef* and *Flat* values; while WinDesign optimizes these values to maximize the boat speed for a given wind condition, the developed VPP is more flexible in that it allows the user to input *Reef* and *Flat* values to mimic how they would sail the boat. In this respect the developed VPP is better at helping a designer create a yacht given a basic understanding of trimming sails whereas WinDesign is more suited to instructing a sailor how to sail a specific boat in order to maximize performance. When the optimized values from WinDesign VPP are used with the developed VPP, the results are even closer though at the expense of smooth trends with respect to heel and

leeway angles. These trends, though less than intuitive, match those of WinDesign VPP, further supporting the validity of the developed VPP. Ultimately, these trends illustrate that WinDesign VPP prioritizes optimizing speed (which may occasionally provide less realistic results regarding heel and leeway angles) whereas in seeking to minimize the differences between opposing forces equally the developed VPP optimizes performance in a more holistic manner.

The modification of the VPP to accept foiling watercraft makes the program significantly more flexible but also hinders the ability to validate results as there were no four degree of freedom VPPs available to compare results to. However, the results from the program can still be verified by comparing the predicted performance of different hullforms with and without foils. Taking into consideration the effective span of foils as determined by tow tank testing at Solent University, a rudimentary foil was added to the previously analyzed Farr 52' hull. As expected, the addition of a foil had a negligible effect on the performance of the yacht with vertical lift and righting moment gains negated by increases in resistance due to greater wetted surface areas. Fundamentally, this is due to the nature of the Farr 52' whose hullform takes advantage of heeling through a reduction of wetted surface area and a displacement typical of boats designed before lifting foils were conceivable. When those same foils were outfitted onto a Lazare Open 60 which is a more modern, albeit larger (thus reducing the proportional effect of the foils), racing yacht the results are more dramatic. With a significantly lighter displacement the foils are able to have a great impact in the total righting moment of the vessel and are able to sufficiently lift the boat out of the water to reduce resistance. Unsurprisingly, this sailboat was designed with the expectation that it would sail with foils and has a hullform that is well adapted to taking advantage of the benefits they provide. The effects of the foils are further emphasized by exaggerating their spans to lengths more commonly seen in similar boats (such as the IMOCA 60 class). Notably, increasing the span, and thus the lifting surface of the foil, not only provides greater speed gains in high beam winds (where the foils are most effective) but they also further decrease performance at low speeds with wind off the bow or abaft the beam. This is a logical trend as the larger span creates both more lift but also induces more resistance; thus in wind conditions where the lift generated dominates resistance larger lifting areas exaggerate benefits while in conditions where the resistance is greater

than lifting benefits the increased wetted surface area further penalizes performance. Ultimately, these results agree with modern consensus on the use of foils in sailing: that they are most effective when paired with light boats that sail upright at high speeds.

In order to develop this VPP, a solid understanding of the mechanics of sailing and the theory of hydrodynamics was critical. Only after much research into the historical developments and current ideas of these fields could the foundation of this program be laid. In addition, an intimate grasp of the Delft Systematic Yacht Hull Series and its iterations from conception until present day played a crucial role in developing the resistance model used. These theoretical and mathematical models would have been little use without being able to analyze them using modern computational tools. Competent use of WinDesign VPP was essential to the validation of the three degree of freedom VPP and the introduction of foils to the VPP required a thorough knowledge of the XFOIL program to effectively calculate lift and drag on foil profiles at different angles of attack and Reynolds numbers. Additionally, the modeling of yachts could not have been possible without a mastery of the Maxsurf suite. Developing the VPP demanded a mastery of not only native Excel functions but also learning VBA (Visual Basic for Applications) so as to write efficient macros and create numerous User Define Functions. Over the course of several months, numerous different versions of the VPP were created, each building off previous versions adding functionality, fixing bugs, and improving results. Finally, multiple weeks of tow tank testing were conducted to validate VPP inputs and verify results. In all, the development of this VPP combined theoretical formulae with computational modelling and physical testing to create the program in its current state.

This project provides plenty of opportunities for further research. Currently the VPP is only suited for upwind sailing as it lacks spinnaker inputs and calculations. Though differently shaped from main and jib sails the mechanics behind how spinnaker sails works is the fundamentally the same as for other types of sails. The main complication with including down wind sailing in the VPP is determining the transition from upwind to downwind sailing regimes. Logically this point ought to be at the intersection of the upwind polar curve with the downwind one, that is, when the true wind angle where the jib and main provide the same speed as the spinnaker and main. Within the current

framework of the VPP this shouldn't be difficult to implement but would likely require some creativity for efficient implementation. Similarly, the sail area calculation for the jib and main could be improved. Currently the VPP calculates these areas by assuming triangular sails with a percentage added to account for the roach. However, currently the Offshore Racing Congress (ORC 2023) uses a more accurate method for determining sail areas (used for handicapping boats) that better estimates areas based on a greater number of sail measurements. While improving accuracy, the greatly increased number of inputs also hinders the ease of use of the VPP, especially early in the design process when sails have not yet been cut or fully sized. Therefore, implementing the option to use either the standard, legacy sail area calculations (as currently in use) or the ORC calculations would provide both the benefits of the improved accuracy while retaining the current ease of use.

More substantially, since the current VPP is largely based off the regressions of the Delft Systematic Yacht Hull Series it is also bounded by the constraints of those regressions. While the original parent hull of the series no longer resembles current sailing hulls, follow on parent hulls have expanded the hull parameters for which the series is valid, extending its usage to more modern style hulls. However, the speed regime for which the models have been tested still lags significantly behind modern boats. While regression lines for upright resistance have been formulated for up to a Froude number of 0.75, all other trends stop at 0.6, which while sufficient for older sail boats as it equates to a boat speed of 14 knots (7.18 m/s) for the Farr 52' is only equal to 14.9 knots (7.65 m/s) for and IMOCA Open 60, well slower than their cruising speeds. Thus, perhaps the greatest handicap of this VPP is its inherent inability to predict realistic boat speeds for foiling yachts. Though broad in scope an extension of all the regression lines to much high Froude numbers would likely have the greatest impact on improving the scope of this VPP.

8 APPENDIX

The following sections provide supplemental information and more comprehensive explanations of ideas and concepts posed in this thesis. The first three sections detail environmental parameters and specifics of the yacht hulls and sail models used in tow tank testing and VPP analyses. The next three sections provide more thorough explanations and derivations of the mathematical models used to calculate forces and moments. The final two sections describe the Excel User Defined Functions and macro that were developed to automate the developed VPP.

8.1 Environmental Parameters

Listed below are the environmental parameters used for processing the tow tank data and VPP calculations. The tow tank values correspond to those of fresh water at 15 degrees Celsius whereas the VPP values are those of saltwater for which a sailboat is expected to sail in.

Parameter		Full Scale	
Tow Tank	g	9.81	m/s^2
	ρ	1000	kg/m^3
	μ	0.00114	$Pa*s$
VPP	g	9.81	m/s^2
	ρ	1025	kg/m^3
	ρ_a	1.293	kg/m^3
	μ	0.00119	$Pa*s$

Table 2: Environmental parameters

8.2 Farr 52' Principle Characteristics

The following section describes the principle characteristics of the Farr 52' yacht used throughout this paper as well as a proposed sailing rig. The model parameters describe the physical model that was used for tow tank testing at Solent University's Hydrodynamics Centre whereas the full scale parameters were used in the VPP (in order to avoid computational issues with small Reynolds numbers associated with model sized foil attachments).

8.2.1 Hull Parameters

The hull parameters, listed in Table 3, are those of the Farr 52' bare hull, that is, the hull without any appendages (such as the keel or rudders).

Parameter	Model		Full Scale	
L_{OA}	2.2642	m	15.85	m
L_{WL}	2.0853	m	14.60	m
B_{WL}	0.4886	m	3.42	m
T_c	0.07	m	0.49	m
∇_c	0.029012	m ³	10.8	m ³
C_p	0.536	–	0.536	–
LCB	55.59	%	55.59	%
S_c	0.7831	m ²	36.2	m ²
$1 + k$				

Table 3: Farr 52' hull parameters

8.2.2 Keel Parameters

Listed in Table 4 are the parameters that define the fin keel used on the Farr 52 model that was tow tank tested.

Parameter	Model		Full Scale	
	V_K	0.000314	m ³	0.11
Root Chord	0.1286	m	0.9002	m
Tip Chord	0.0964	m	0.6748	m
Span	0.367	m	2.569	m
t/c ratio	10	–	10	–
Chord _{Avg}	0.1125	m	0.788	m
S_K	0.082575	m ²	4.0462	m ²
$1 + k$	1.206	–	1.206	–

Table 4: Keel parameters

8.2.3 Bulb Parameters

Table 5 lists the parameters of the keel bulb outfitted on the Farr 52' model.

Parameter	Model		Full Scale	
	∇_b	0.00006559	m ³	0.225
Profile t/c	15.2	–	15.2	–
Plan t/c	26	–	26	–
t/c ratio _{Avg}	0.206	–	0.206	–
S_c	0.00101	m ²	0.0496	m ²
$1 + k$	1.309	–	1.309	–

Table 5: Bulb parameters

8.2.4 Sail Parameters

The dimensions and parameters of the sail set used for the VPP analysis of the Farr 52' are listed in Table 6. Since the VPPs analyze the full scale yacht, the sails are also full sized and the individual parameters are defined in Figure 27.

For the given wind default wind conditions (true wind speeds between 10 and 20 knots), in order to mimic how a sailor would typically trim this sail set a constant *Reef* value of 0.9 was chosen in conjunction with a *Flat* value that progressively decreases from 0.9 to

Parameter		Full Scale	
Main	P	20	m
	E	7	m
	BAD	1.6	m
	Roach	10	%
Jib	I	18.7	m
	J	6	m
	Lpp	7.56	m
	Roach	0	%

Table 6: Sail set parameters

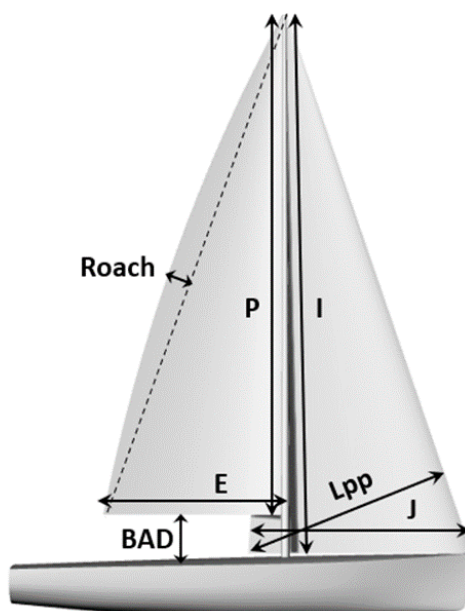


Figure 27: Definition of sail set parameters

0.6 as the wind strength increases.

8.3 Lazare Open 60 Principle Characteristics

The Lazare Open 60 is a racing yacht which adheres to the IMOCA Open 60 class rules. Originally designed as a foiling yacht as a part of Lazare Gournay's master thesis (Gournay 2022) and research at Solent University it has been utilized as a test hull for VPP analysis

for which its hull and appendage parameters are listed in Table 7.

Parameter		Full Scale	
Hull	Δ	8.385	t
	Ballast Ratio	0.335	–
	LOA	18.28	m
	L_{WL}	16.58	m
	B_{OA}	5.60	m
	B_{WL}	4.11	m
	T_c	0.31	m
	C_p	0.64	m
	LCF	56.15	%
	LCB	60.56	%
Keel	Root Chord	0.76	m
	Root t/c	0.1	–
	Tip Chord	0.40	m
	Tip t/c	0.15	m
	Span	3.815	m
	V_k	0.10	m ³
Bulb	V_{bulb}	0.22	m ³
	Chord	2.7	m
	ρ_{bulb}	11343	kg/m ³
	WSA	2.24	m ²
	t/c Avg	0.15	–
Rudder	#	1	–
	Root Chord	0.580	m
	Root t/c	0.1	–
	Tip Chord	0.18	m
	Tip t/c	0.11	m
	Span	2	m
	ρ	2000	kg/m ³

Table 7: Lazare Open 60 principle characteristics

8.4 Sail Calculations

8.4.1 Sail Areas

Based on the sail parameters listed in Table 6 and the definitions of the various sail parameters illustrated in Figure 27 the areas of the the main sail, SA_{Main} , and the jib sail, SA_{Jib} , can be calculated as:

$$SA_{Main} = \frac{1}{2}(P \times E) \times Roach$$

$$SA_{Jib} = \frac{1}{2}L_{pp}\sqrt{I^2 + J^2} \times Roach$$

8.4.2 Centers of Effort

Though modern sails are somewhat triangular in shape, due to their complex geometry and the variation in lift across the height of a sail due to changes in camber and twist the center of effort of a sail is often approximated as 39% of the height of a sail (Barkley, personal communication). Since reefing shortens a sail, the *Reef* reduction factor is included in the center of effort calculations as well as the height of the freeboard and BAD since the foot of the sails are located at the deck and boom (for jib and main sails respectively) and not the waterline.

$$Z_{e,Main} = 0.39 \times P \times Reef + (BAD + Freeboard)$$

$$Z_{e,Jib} = 0.39 \times I \times Reef + (Freeboard)$$

8.5 Delft Systematic Yacht Hull Series Coefficients

The first hulls of the Delft Systematic Yacht Hull Series were developed and tank tested in 1973 as a collaboration between Delft University and the Massachusetts Institute of Technology with the aim of developing design tools to assist in the creation of VPPs. In 1975 the first paper was published as a part of this project and presented best fit regressions for upright resistance for the first nine systematic hull models for speeds up to a Froude number of 0.45. The second formulation of this series was Gerritsma, Onnick, and

Versluis 1981 which also tested the models to a Froude number of 0.45 but expanded the set of models to twenty two hull (all based off the parent hullform) establishing what is known as Series 1. Due to the considerably larger set of hulls more parameters could be tested and the regression lines could be fit with better confidence. In 1987 a new parent hullform was created to better represent modern sailing vessels and through varying parameters of this parent model Series 2 was created which contained six unique hulls. These models were tested up to Froude number 0.60 which required a second set of regressions for the higher speed runs due to planing phenomena. This second set of approximations created discontinuities at the transition (around Froude number 0.45) which were resolved by Gerritsma, Keuning, and Onnick 1993 with the creation of Series 3 which contained eleven new models based off a third parent hull. Due to better understanding of sailing mechanics (in part due to the experimentation at the Delft Ship Hydromechanics Laboratory) and improvements in materials technology there was a trend towards more efficient keels and rudders with higher aspect ratios that no longer resembled the original appendages fitted on the first three series hullforms. To remedy this, Series 4 was created, being the total number of hulls within the Delft systematic series to fifty, with its own series of keels and rudders. Keuning and Sonnenberg 1999 introduced the concept of bare hull resistance to accommodate varying appendage forms and presented regressions based off Series 4 and reformulations of the previous three series without appendages. Notably, these reformulations enabled smooth transitions between data sets and coupled each trend with the displacement-length ratio so that they, in a manner of speaking, became weight dependant. Since 1998, in an effort to keep up with the evolution of sailboat design, six new models were added forming Series 6 and 7. These newest models plus various high speed hullforms from the previous models have since been tested up to Froude number 0.75, though the incomplete nature of the testing data set and resulting regressions have left them partially functional.

Table 8 lists the parameters that define the Delft Systematic Yacht Hull Series and the minimum and maximum values that bound the hulls tested. Hence, this table describes the boundary conditions that constrain the regression lines presented in this section.

Parameter	Min	Max	Nomenclature
L_{WL}/B_{WL}	2.73	5.00	Length - Beam ratio
B_{WL}/T_c	2.46	19.38	Beam - Draft ratio
$L_{WL}/V_c^{1/3}$	4.34	8.50	Length - Displacement ratio
LCB	-8.2%	0.0%	Long'l center of Buoyancy
LCF	-9.5%	-1.8%	Long'l Center of Flotation
C_p	0.52	0.60	Prismatic coefficient
C_m	0.65	0.78	Midship Area coefficient
$A_W/V_c^{2/3}$	3.78	12.67	Loading Factor

Table 8: Delft Systematic Yacht Hull Series parameters

The following sub-sections contain the regressions developed from the Delft Systematic Yacht Hull Series, primarily from Keuning and Sonnenberg 1999, as well as their respective tables of coefficients.

8.5.1 Upright Residuary Resistance

Canoe Body

Based on numerous tow tank tests at Delft University and building off much of the work of Gerritsma and his colleagues Keuning and Sonnenberg 1999 developed a regression to determine the bare hull upright residuary resistance for hullforms that fall within the Delft Systematic Yacht Hull Series parameters. The following formulation and respective table of coefficients are what they derived from experimental data.

$$C_{r,c} = a_0 \left(a_1 \frac{LCB}{L_{WL}} + a_2 C_p + a_3 \frac{\nabla_c^{2/3}}{A_W} + a_4 \frac{B_{WL}}{L_{WL}} \right) \frac{\nabla_c^{1/3}}{L_{WL}} + \left(a_5 \frac{\nabla_c^{2/3}}{S_c} + a_6 \frac{LCB}{LCF} + a_7 \left(\frac{LCB}{LCF} \right)^2 + a_8 C_p^2 \right) \frac{\nabla_c^{1/3}}{L_{WL}}$$

Fn	a_0	a_1	a_2	a_3	a_4	a_5	a_6	a_7	a_8
0.1	-0.0014	0.0403	0.0470	-0.0227	-0.0119	0.0061	-0.0086	-0.0307	-0.0553
0.15	0.0004	-0.1505	0.1793	-0.0004	0.0097	0.0118	-0.0055	0.1721	-0.1728
0.2	0.0014	-0.1071	0.0637	0.0090	0.0153	0.0011	0.0012	0.1021	-0.0648
0.25	0.0027	0.0463	-0.1263	0.0150	0.0274	-0.0299	0.0110	-0.0595	0.1220
0.3	0.0056	-0.8005	0.4891	0.0269	0.0519	-0.0313	0.0292	0.7314	-0.3619
0.35	0.0032	-0.1011	-0.0813	-0.0382	0.0320	-0.1481	0.0837	0.0223	0.1587
0.4	-0.0064	2.3095	-1.5152	0.0751	-0.0858	-0.5349	0.1715	-2.4550	1.1865
0.45	-0.0171	3.4017	-1.9862	0.3242	-0.1450	-0.8043	0.2952	-3.5284	1.3575
0.5	-0.0201	7.1576	-6.3304	0.5829	0.1630	-0.3966	0.5023	-7.1579	5.2534
0.55	0.0495	1.5618	-6.0661	0.8641	1.1702	1.7610	0.9176	-2.1191	5.4281
0.6	0.0808	-5.3233	-1.1513	0.9663	1.6084	2.7459	0.8491	4.7129	1.1089

Table 9: Canoe body upright residuary resistance coefficients

Keel

Similarly, the upright residuary resistance due to the keel can be calculated using the regression and coefficients determined by Keuning and Sonnenberg 1999. Notably, there are no coefficients for Froude numbers below 0.2 in Table 10 as at such low speeds the wave trough generated along the length of a sailboat's hull is not great enough for the keel to influence wave generation (and thus residuary resistance).

$$C_{r,k} = A_0 + A_1 \frac{T}{B_{WL}} + A_2 \frac{T_c + Z_{cbk}}{\nabla_k^{\frac{1}{3}}} + A_3 \frac{\nabla_c}{\nabla_k}$$

8.5.2 Heeled Wetted Surface Area

The formula for the wetted surface area of the Delft Systematic Yacht Hull Series was originally proposed in Gerritsma, Keuning, and Onnick 1993 and was later revised by Keuning and Sonnenberg 1999 to account for the extension of the systematic series.

$$S_c = \left(1.97 - 0.171 \frac{B_{WL}}{T_c}\right) \left(\frac{0.65}{C_m}\right)^{\frac{1}{3}} (\nabla_c L_{WL})^{\frac{1}{2}}$$

Fn	A_0	A_1	A_2	A_3
0.1				
0.15				
0.2	-0.00104	0.00172	0.00117	-0.00008
0.25	-0.00550	0.00597	0.00390	-0.00009
0.3	-0.01110	0.01421	0.00069	0.00021
0.35	-0.00713	0.02632	-0.00232	0.00039
0.4	-0.03581	0.08649	0.00999	0.00017
0.45	-0.00470	0.11592	-0.00064	0.00035
0.5	0.00553	0.07371	0.05991	-0.00114
0.55	0.04822	0.00660	0.07048	-0.00035
0.6	0.01021	0.14173	0.06409	-0.00192

Table 10: Keel upright residuary resistance coefficients

Also published in Keuning and Sonnenberg 1999 is the formulation for the wetted surface area of a heeled hullform which is based off the upright wetted surface area multiplied by a factor that is a function of the hull parameters and the table of coefficients listed in Table 11 below.

$$S_{c,\phi} = S_c \left(1 + \frac{1}{100} \left(s_0 + s_1 \frac{B_{WL}}{T_c} + s_2 \left(\frac{B_{WL}}{T_c} \right)^2 + s_3 C_m \right) \right)$$

ϕ	s_0	s_1	s_2	s_3
0	0	0	0	0
5	-4.112	0.054	-0.027	6.329
10	-4.522	-0.132	-0.077	8.738
15	-3.291	-0.389	-0.118	8.949
20	1.850	-1.200	-0.109	5.364
25	6.510	-2.305	-0.066	3.443
30	12.334	-3.911	0.024	1.767
35	14.648	-5.182	0.102	3.497

Table 11: Heeled wetted surface area coefficients

8.5.3 Heeled Residuary Resistance

Canoe Body

The following formula and table of coefficients, derived from experimental data by Keuning and Sonnenberg 1999, enable the calculation of the change in residuary resistance of the bare hull due to changes in heel. There are no coefficients for low Froude numbers in Table 12 as at such low speeds there are negligible changes in the residuary resistance as most of the drag is dominated by viscous resistance (and its changes due to heeling).

$$\Delta R_{r,h,\phi=20} = \nabla_c \rho g \left(u_0 + u_1 \frac{L_{WL}}{B_{WL}} + u_2 \frac{B_{WL}}{T_c} + u_3 \left(\frac{B_{WL}}{T_c} \right)^2 + u_4 LCB + u_5 LCB^2 \right)$$

Keel

As with the bare hull, Keuning and Sonnenberg 1999 noted that when heeled there was a change in the residuary resistance due to the presence of the keel which can be approximated by the following equation and coefficients listed in Table 13.

$$Ch = H_1 \frac{T_c}{T} + H_2 \frac{B_{WL}}{T_c} + H_3 \frac{T_c}{T} \frac{B_{WL}}{T_c} + H_4 \frac{L_{WL}}{\nabla_c^{\frac{1}{3}}}$$

Fn	u_0	u_1	u_2	u_3	u_4	u_5
0.1						
0.15						
0.2						
0.25	-0.0268	-0.0014	-0.0057	0.0016	-0.0070	-0.0017
0.3	0.6628	-0.0632	-0.0699	0.0069	0.0459	-0.0004
0.35	1.6433	-0.2144	-0.1640	0.0199	-0.0540	-0.0268
0.4	-0.8629	-0.0354	0.2226	0.0188	-0.5800	-0.1133
0.45	-3.2715	0.1372	0.5547	0.0268	-1.0064	-0.2026
0.5	-0.1976	-0.1480	-0.6593	0.1862	-0.7489	-0.1648
0.55	1.5873	-0.3749	-0.7105	0.2146	-0.4818	-0.1174
0.6						

Table 12: Canoe body heeled residuary resistance coefficients

H_1	H_2	H_3	H_4
-3.5837	-0.0518	0.5958	0.2055

Table 13: Keel heeled residuary resistance coefficients

8.5.4 Effective Draft of Keel

Once again building off the work of Gerritsma, Keuning, and Onnick 1993, Keuning and Sonnenberg 1999 expanded the scope of the effective keel draft calculation to take into account changes in Froude number of the vessel (which explains the use of the B variables) and further adjusted the tabulated coefficients, listed in Table 14, to best fit the extended hull series.

$$T_E = T \left(A_1 \frac{T_c}{T} + A_2 \left(\frac{T_c}{T} \right)^2 + A_3 \frac{B_{WL}}{T_c} + A_4 T_R \right) (B_0 + B_1 Fn)$$

ϕ	A_1	A_2	A_3	A_4	B_0	B_1
0	3.7455	-3.6246	0.0589	-0.0296	1.2306	-0.7256
10	4.4892	-4.8454	0.0294	-0.0176	1.4231	-1.2971
20	3.9592	-3.9804	0.0283	-0.0075	1.5450	-1.5622
30	3.4891	-2.9577	0.0250	-0.0272	1.4744	-1.3499

Table 14: Effective draft coefficients

8.5.5 Keel Side Force

Originally developed in Gerritsma, Onnick, and Versluis 1981; Gerritsma, Keuning, and Onnick 1993 reformulated the keel side force approximation to better model the then expanded systematic series. Though the series expanded again, Keuning and Sonnenberg 1999 continued to use the same equation and coefficients (Table 15) as published in Gerritsma, Keuning, and Onnick 1993.

$$KSF(\phi) = \beta \frac{1}{2} \rho V^2 S_c \left[b_1 \frac{T^2}{S_c} + b_2 \frac{T^4}{S_c^2} + b_3 \frac{T_c}{T} + b_4 \frac{T_c \times T}{S_c} \right]$$

ϕ	b_1	b_2	b_3	b_4
0	2.025	9.551	0.631	-6.575
10	1.989	6.729	0.494	4.745
20	1.980	0.633	0.194	-0.792
30	1.762	-4.957	-0.087	2.766

Table 15: Keel side force coefficients

8.6 Foil Calculations

The following section describes the derivation of the equations based on those proposed by Gournay 2022 used to determine the lift, drag, and side force generated by submerged foils as well as the apparent leeway and angle of attack of the inclined foils. To aide in the explanation of the derivation process and explain definitions Professor Giles Barkley of Solent University provided the figures used in this section though theses figures have been edited for clarity and to maintain a consistent use of variables.

8.6.1 Calculating Apparent Flow Velocity and Angle of Attack

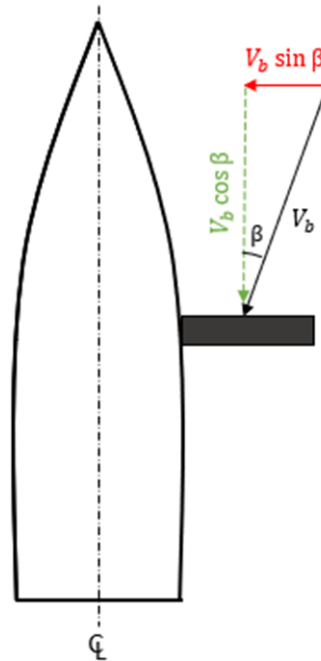


Figure 28: Calculation of apparent flow speed - plan view

Assuming that a boat sails with a velocity V_b at a leeway angle β , then as shown in Figure 28 the apparent flow velocity parallel and perpendicular to the centerline of the boat are given by:

$$\begin{cases} V_b \times \cos \beta & \text{Parallel} \\ V_b \times \sin \beta & \text{Perpendicular} \end{cases}$$

Considering the boat heeled to an angle of ϕ degrees and the foil inclined at an angle of α degrees, within the three dimensional context, relative to the foil the parallel and perpendicular flow vectors can be illustrated as in Figure 29.

In Figure 29 the $V_b \times \cos \beta$ and $V_b \times \sin \beta$ plane remains parallel to the waterplane while the foil is angled at $(\phi + \alpha)$ degrees from the waterline. Then, the velocity of the boat perpendicular to the foil (solid red line) can be defined as:

$$V_{b,\perp} = V_b \times \sin \beta \times \sin (\phi + \alpha)$$

The apparent velocity of oncoming water with respect to a submerged foil, V_f , is a function of the leeway angle of the boat as well as the sum of the heel of the boat and the heel of

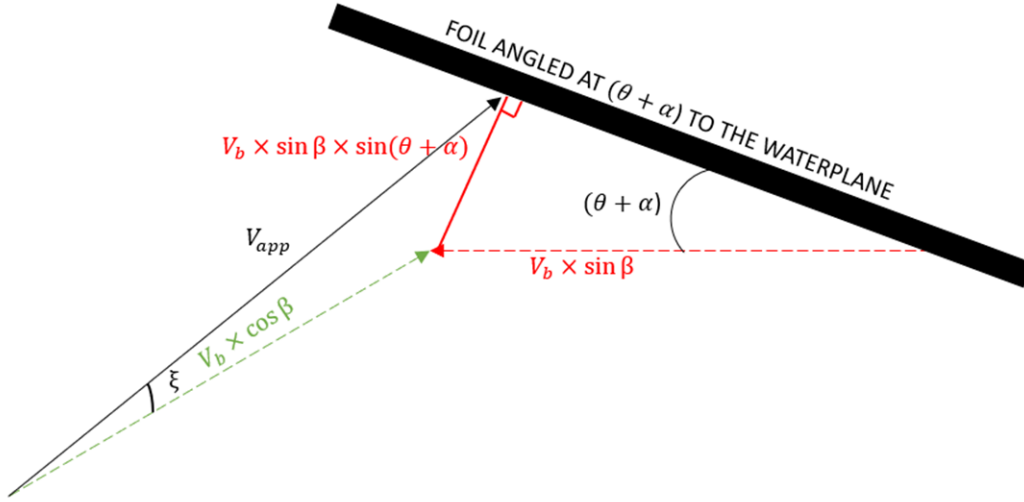


Figure 29: Calculation of apparent flow speed

the foil itself and thus can be written as:

$$V_f = V_{app} = \sqrt{V_b \times (\sin \beta \sin (\phi + \alpha))^2 + (V_b \times \cos \beta)^2}$$

which, when simplified, describes the apparent velocity as a function of the boat speed:

$$V_f = V_{app} = V_b \sqrt{(\sin \beta \sin (\phi + \alpha))^2 + (\cos \beta)^2}$$

The apparent angle of attack in the plane perpendicular to the foil section, ξ , can be expressed in terms of the boat velocity resolved perpendicular to the foil and parallel to the ship's centerline as:

$$\xi = \tan^{-1} \left(\frac{V_b \times \sin \beta \times \sin (\phi + \alpha)}{V_b \times \cos \beta} \right)$$

Notably, the V_b terms cancel out leaving the equation solely in terms of angles and the $\left(\frac{\sin \beta}{\cos \beta} \right)$ can be rewritten in terms of $\tan \beta$ leading to the simplified equation:

$$\xi = \tan^{-1} (\tan \beta \times \sin (\phi + \alpha))$$

A closer inspection of Figure 29 reveals that the apparent flow speed generates an apparent leeway angle. Expanding on this, Figure 30 reflects the correction that must be made to the leeway angle.

The apparent leeway angle of the foil with respect to the oncoming flow is the leeway angle of the vessel as a whole, β , corrected by the leeway modification factor, η , which

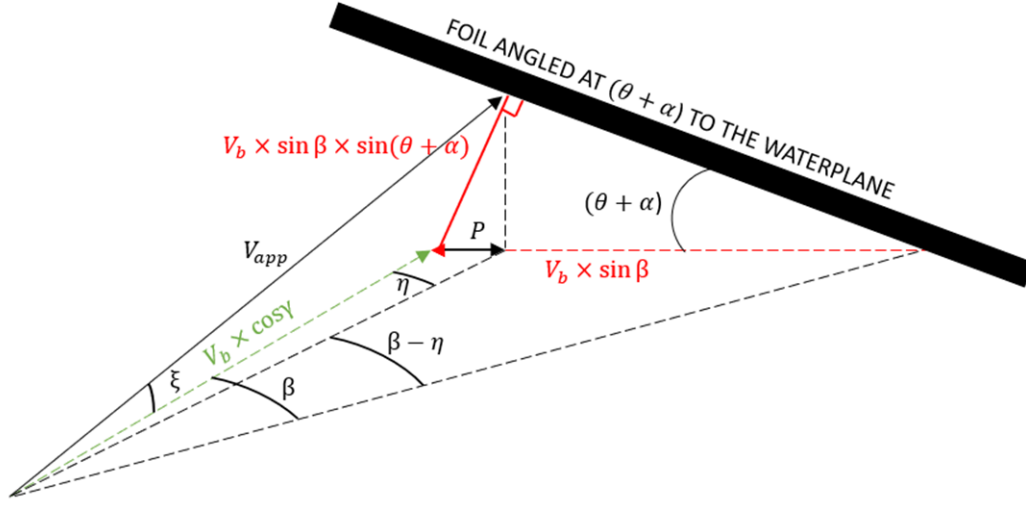


Figure 30: Calculation of apparent leeway angle

can be calculated as:

$$\eta = \tan^{-1} \left(\frac{P}{V_b \times \cos \beta} \right) \quad \text{where} \quad P = V_b \times \sin \beta \times \sin(\phi + \alpha) \times \sin(\phi + \alpha)$$

Where P , the projection of η onto the component of velocity parallel to the foil span, is defined in terms of the velocity perpendicular to the foil and the angle $(\phi + \alpha)$. Thus, through simplification, η can be rewritten as:

$$\eta = \tan^{-1} (\tan \beta \times \sin^2(\phi + \alpha))$$

8.6.2 Calculating Lift and Drag Forces

Next, based on the calculated apparent angle of attack of the foil lift and drag forces can be determined as illustrated in Figure 31.

Since the lift and drag generated by a foil are calculated relative to the position of the foil, they must be rotated by the apparent angle of attack. Resolving the lift, $L_{section}$, and drag, $D_{section}$, orthogonally to the waterplane leads to the following equations:

$$\begin{cases} L_{\perp span} = L_{section} \times \cos \xi - D_{section} \times \sin \xi \\ D_{\parallel flow} = L_{section} \times \sin \xi + D_{section} \times \cos \xi \end{cases}$$

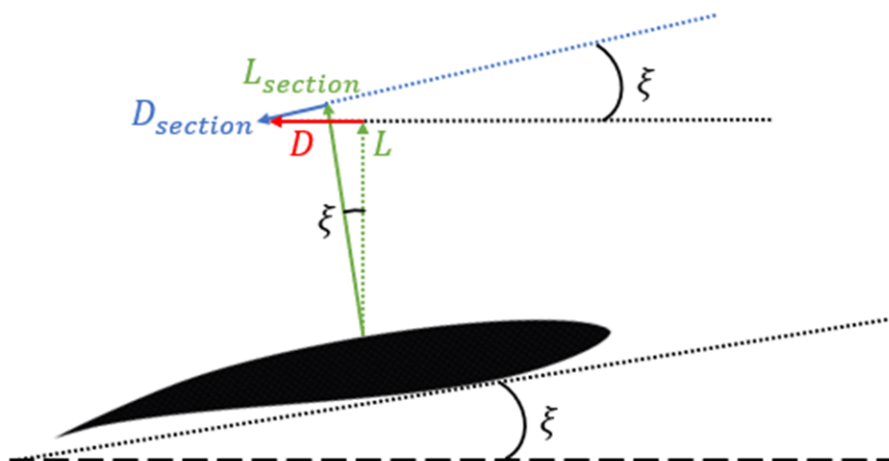


Figure 31: Lift and drag forces

Resolving Lift and Side Force

As illustrated in Figure 32 the lift calculated is perpendicular to the span of the foil. The vertical component of the lift generated can be found by projecting the calculated lift onto the ship's frame of reference.

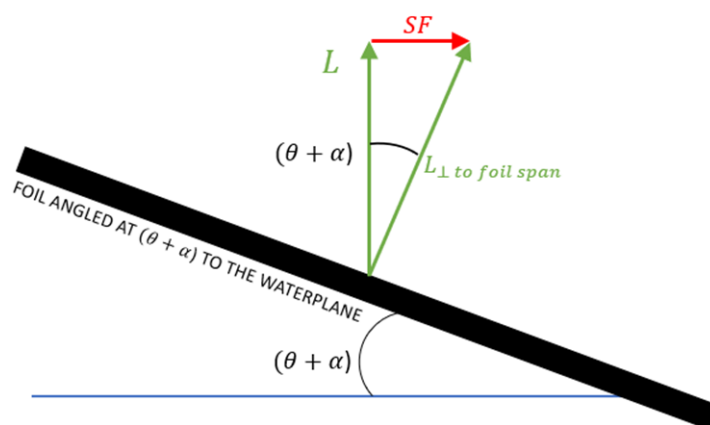


Figure 32: Lift and side forces

Projecting the lift calculated onto the vertical plane yields the lift, in the ship's frame of reference as:

$$L = (L_{section} \times \cos \xi - D_{section} \times \sin \xi) \times \cos (\phi + \alpha)$$

This then introduces the side force which is the result of the projection of the lift generated by the foil onto the horizontal waterplane. Thus the side force generated by the foil can be described as:

$$SF = (L_{section} \times \cos \xi - D_{section} \times \sin \xi) \times \sin (\phi + \alpha)$$

Resolving Drag

Since the drag calculated is in the direction of the in flow velocity which is at an angle $(\beta - \eta)$ to the ship's centerline this drag force must be rotated to the ship's frame of reference.

$$D = D_{\parallel flow} \times \cos (\beta - \eta)$$

which can then be expanded as

$$D = (L_{section} \times \sin \xi + D_{section} \times \cos \xi) \times \cos (\beta - \eta)$$

Thus, the lift, drag, and side forces generated by the submerged foil with respect to the global frame of reference can be written as:

$$\begin{cases} L &= (L_{section} \times \cos \xi - D_{section} \times \sin \xi) \times \cos (\phi + \alpha) \\ SF &= (L_{section} \times \cos \xi - D_{section} \times \sin \xi) \times \sin (\phi + \alpha) \\ D &= (L_{section} \times \sin \xi + D_{section} \times \cos \xi) \times \cos (\beta - \eta) \end{cases}$$

8.7 Excel Lambda Functions

In 2020 Microsoft introduced the Lambda function in Excel, allowing the creation of UDFs (User Defined Functions) without the use of VBA or Macros; instead, UDFs could be written as any other formula in a worksheet cell, stored as a named value within Name Manager and then called as a function. Custom functions created in this manner can be used across the entire workbook while the logic exists in one place, increasing the flexibility of formulae usage and reducing error troubleshooting (as corrections to the UDF are automatically integrated into every usage of the function).

Lambda functions have the syntax: =LAMBDA(parameter, parameter, ... , calculation)

8.7.1 Array of Integer Divisors

To calculate the arrays for true wind speed and angle divisions the following Lambda function was written. This function is used in data validation to ensure even divisions of a data set without remainders (such as for divisions of true wind speeds and angles).

In Excel, the Let function enables a user to define named variables within a formula. This capability can make the formulae more readable and reduces redundant calculations.

= LAMBDA(Min, Max, LET(d, (Max - Min), array, IF(MOD(d, SEQUENCE(d, 1)) = 0, SEQUENCE(d, 1), 0), FILTER(array, array <> 0)))

8.7.2 True Wind Arrays

True Wind Speed

To create a repeating array of the true wind speeds for each true wind angle value the following function was developed. In effect, it counts up from the minimum wind speed, TWS_{Min} , to the maximum wind speed, TWS_{Max} , (by predetermined increments, TWS_{inc}) in modulo number of wind speed increments. It does this for each true wind angle, after which it terminates the array.

= MOD(SEQUENCE((1 + (TWA_{Max} - TWA_{Min})/TWA_{inc}) * (1 + (TWS_{Max} - TWS_{Min})/TWS_{inc}), 1, 0, TWS_{inc}), (TWS_{Max} - TWS_{Min} + TWS_{inc})) + TWS_{Min}

True Wind Angle

To create an array of true wind angles that compliments the true wind speed array such that every unique combination of wind speed and angle is accounted for the following function was devised. Effectively this function creates an array of values between the minimum true wind angle, TWA_{Min} , and the maximum, TWA_{Max} , which are then rounded down to the nearest true wind angle by the floor function so as to create groupings of wind angles for each set of true wind speeds.

= FLOOR(SEQUENCE((1 + (TWA_{Max} - TWA_{Min})/TWA_{inc}) * (1 + (TWS_{Max} - TWS_{Min})/TWS_{inc}),

$1, 0, 1/((TWS_{Max} - TWS_{Min})/TWS_{inc} + 1), 1) * TWA_{inc} + TWA_{Min}$

8.7.3 Linear Interpolation

Since there is no native linear interpolation formula in Excel to be able to efficiently interpolate values between known points the following User Defined Function was written. This linear interpolation function works in two parts. The first part is an *if* statement that determines whether or not the target input value matches a known input value (such as from a provided table of input and output values); if so the known output value is assigned, if not the the second part of the function is executed. This first part is included so as to prevent any divide by zero errors that may occur. The second part determines the nearest known input values to the desired input value, calculates the relative position of the desired input value with respect to the nearest tabulated values, and determines the appropriate output value based on a weighted average determined by the relative position. This function makes use of Excel's Let function which allows standard excel terminology with more concise variables.

```
= LAMBDA(lookup_value, lookup_array, return_array, LET(t, lookup_value, xarray, lookup_array,
yarray, return_array, IF((XLOOKUP(t, xarray, xarray,, 1)-XLOOKUP(t, xarray, xarray,, -1)) = 0, XLOOKUP(t, xarray, yarray,, 0), ((XLOOKUP(t, xarray, yarray,, 1) -
XLOOKUP(t, xarray,yarray,, -1))/(XLOOKUP(t, xarray, xarray,, 1) - XLOOKUP(t, xarray, xarray,, -1)) * (t - XLOOKUP(t, xarray, xarray,, -1)) + XLOOKUP(t, xarray, yarray,,
-1))))))
```

8.7.4 Bilinear Interpolation

Bilinear interpolation of array f with respect to values x^* and y^* is given by:

$$f(x^*, y^*) = \frac{1}{(x_2 - x_1)(y_2 - y_1)} \begin{bmatrix} x_2 - x^* & x^* - x_1 \end{bmatrix} \begin{bmatrix} f(x_1, y_1) & f(x_1, y_2) \\ f(x_2, y_1) & f(x_2, y_2) \end{bmatrix} \begin{bmatrix} y_2 - y^* \\ y^* - y_1 \end{bmatrix}$$

where the subscripts 1 and 2 represent the nearest discrete values neighboring x^* and y^* in array f . The first term in this equation normalizes the expression by the "area" bounded by the nearest x and y neighbors. The second and forth terms express how close the x^* and y^* values are to their neighbors while the third term is the array values at the nearest

neighbors. Since Excel does not permit manipulation of individual values within an array, the second the third terms are post- and pre-multiplied by the permutation matrix, $\begin{bmatrix} 0 & 1 \\ 1 & 0 \end{bmatrix}$, for convenience so that their respective values come from ascending array positions. Thus, the bilinear interpolation equation becomes:

$$f(x^*, y^*) = \frac{1}{(x_2 - x_1)(y_2 - y_1)} \begin{bmatrix} x^* - x_1 & x_2 - x^* \end{bmatrix} \begin{bmatrix} 0 & 1 \\ 1 & 0 \end{bmatrix} \begin{bmatrix} f(x_1, y_1) & f(x_1, y_2) \\ f(x_2, y_1) & f(x_2, y_2) \end{bmatrix} \begin{bmatrix} 0 & 1 \\ 1 & 0 \end{bmatrix} \begin{bmatrix} y^* - y_1 \\ y_2 - y^* \end{bmatrix}$$

Using the Lambda and Let functions the previous expression can be compiled as a User Defined Function as:

```
= LAMBDA(x_target, y_target, x_array, y_array, reference, LET(x, x_target, y, y_target,
xarray, x_array, yarray, y_array, ref, reference, MMULT(MMULT(MMULT(TRANSPOSE(ABS(
OFFSET(ref, XMATCH(y, yarray, -1), 0, 2, 1) - y)), {0,1;1,0}), OFFSET(ref, XMATCH(y,
yarray, -1), XMATCH(x, xarray, -1), 2, 2)), MMULT({0,1;1,0}, TRANSPOSE(ABS(OFFSET(ref,
0, XMATCH(x, xarray, -1), 1, 2) - x)))) * 1/((INDEX(xarray, 1, XMATCH(x, xarray, -
1) + 1) - INDEX(xarray, 1, XMATCH(x, xarray, -1))) * (INDEX(yarray, XMATCH(y,
yarray, -1) + 1, 1) - INDEX(yarray, XMATCH(y, yarray, -1), 1))))))
```

8.8 Excel Macro

The following macro, which is designed to calculate the leeway angle, velocity, and heel angle at a given wind speed and direction, is comprised of two phases. In the first phase, the macro calculates these desired values by progressively changing them until it is able to minimize the sum of the residuals. The program conducts this procedure for the 42 different wind conditions, iterating through $i = 0$ to 41. Due to the non-linear nature of the optimization problem, there may be instances in which the solver used finds a local minimum vice the global minimum. Therefore, a second phase is used to re-initialize the starting point for the optimization problem closer to the global minimum (as determined by solutions at adjacent wind speeds).

To begin the first phase, the indicator cell for each row (cells B25:B66) is set to display "No" with a white background (color index = 0) so as to tell the user that solutions have not yet been found. Next, the Solver add-in is executed for each of the 42 rows. This is accomplished by telling the program to minimize the sum of the residuals, which is the

vertical array starting at $\$S\25 , by changing the values in the vertical arrays starting in cells $\$G\25 , $\$K\25 , and $\$O\25 which correlate to the yacht's leeway angle, velocity, and heel angle, respectively. Constraints that the Froude number (vertical array starting at cell $\$A\25) must be between 0.1 and 0.6, the leeway angle must be less than 10, and the heel angle must be between 0 and 35 degrees are stipulated to bound the feasible region. The solver then iterates through minimizing the sum of the residuals for each row, changing the indicator cell to display "Yes" when complete. If the sum of the residuals for a given row is greater than 0.05 (or there is an error which would display "N/A") then the respective indicator cell will turn red (color index = 3) to notify the user of the invalid solution.

After solving for each row, the second phase begins in which the macro seeks to rectify any solutions which large residuals. For any row where the sum of residuals is greater than 0.05, the macro identifies which residual is the greatest between ε_{SF} , ε_D , and, ε_M ; cells(25 + i , 10), cells(25 + i , 14), and cells(25 + i , 18), respectively, and assigns the position of this value to variable " k ". After identifying which residual is the most egregious, the macro then creates an array of the respective leeway angles, velocities, or heel angles (depending on which residual is the greatest) from the neighboring values calculated for the different wind speeds at the same wind angle. Then, using a linear trend analysis, the macro what value likely should be in position " k ". substituting that new value of leeway, velocity, or heel for the old one the macro then executes the solver again with the same constraints as before. If the new sum of residuals is less than 0.05 the background of the indicator cell then turns white to notify the user of a valid solution. After conducting this process for each sum that is out of tolerance the macro terminates.

```

Sub ResultsSolver()
'
' ResultsSolver Macro
' Solve Results tab by balancing forces.
'
'

Range("B25:B66").Value = "No"
Range("B25:B66").Interior.ColorIndex = 0
' Range("P7").Value = "In Progress"
Dim i As Integer
For i = 0 To 41
    SolverReset
    SolverOk SetCell:=Sheets("Results").Range("$S$25").Offset(i, 0).Address,
MaxMinVal:=2, ValueOf:=0,
ByChange:=Sheets("Results").Range("$G$25,$K$25,$O$25").Offset(i, 0).Address, _
    Engine:=1, EngineDesc:="GRG Nonlinear"
    SolverAdd CellRef:=Sheets("Results").Range("$A$25").Offset(i, 0).Address,
Relation:=3, FormulaText:="0.1" ' Min Fn = 0.1
    SolverAdd CellRef:=Sheets("Results").Range("$A$25").Offset(i, 0).Address,
Relation:=1, FormulaText:="0.6" ' Max Fn = 0.6
    SolverAdd CellRef:=Sheets("Results").Range("$G$25").Offset(i, 0).Address,
Relation:=1, FormulaText:="10" ' Max Leeway angle = 10 deg
    SolverAdd CellRef:=Sheets("Results").Range("$O$25").Offset(i, 0).Address,
Relation:=3, FormulaText:="0" ' Min Heel angle = 0 deg
    SolverAdd CellRef:=Sheets("Results").Range("$O$25").Offset(i, 0).Address,
Relation:=1, FormulaText:="35" ' Max Heel angle = 35 deg
    SolverSolve True
    Cells(25 + i, 2).Value = "Yes"
    If Cells(25 + i, 19) > 0.05 Or Cells(25 + i, 19) = "#N/A" Then
    Cells(25 + i, 2).Interior.ColorIndex = 3
    End If
Next i

Dim j As Integer
Dim k As Integer
Dim xArr(5) As Variant
Dim yArr(5) As Variant

For i = 0 To 41
    If Cells(25 + i, 19) > 0.05 Then
    k = WorksheetFunction.Match(WorksheetFunction.Max(Cells(25 + i, 10), Cells(25 +
i, 14), Cells(25 + i, 18)), Range("A" & 25 + i & ":" & "R" & 25 + i), 0) - 3
    For j = 0 To 5
        xArr(j) = Cells(25 + WorksheetFunction.RoundDown(i / 6, 0) * 6 + j, 3).Value
        yArr(j) = Cells(25 + WorksheetFunction.RoundDown(i / 6, 0) * 6 + j, k).Value
    Next j
    xVal = Cells(25 + i, 3)
    Select Case k

```

```

Case 7
    Cells(25 + i, k) = Application.Trend(yArr, xArr, xVal)
Case 11, 15
    Cells(25 + i, k) = Application.Trend(yArr, xArr, xVal)
End Select
If Cells(25 + i, k) < 0 Then    ' Prevent negative values from trendline
Cells(25 + i, k) = 0
End If
SolverReset
SolverOk SetCell:=Sheets("Results").Range("$S$25").Offset(i, 0).Address,
MaxMinVal:=2, ValueOf:=0,
ByChange:=Sheets("Results").Range("$G$25,$K$25,$O$25").Offset(i, 0).Address, _
    Engine:=1, EngineDesc:="GRG Nonlinear"
    SolverAdd CellRef:=Sheets("Results").Range("$A$25").Offset(i, 0).Address,
Relation:=3, FormulaText:="0.1"    ' Min Fn = 0.1
    SolverAdd CellRef:=Sheets("Results").Range("$A$25").Offset(i, 0).Address,
Relation:=1, FormulaText:="0.6"    ' Max Fn = 0.6
    SolverAdd CellRef:=Sheets("Results").Range("$G$25").Offset(i, 0).Address,
Relation:=1, FormulaText:="10"    ' Max Leeway angle = 10 deg
    SolverAdd CellRef:=Sheets("Results").Range("$O$25").Offset(i, 0).Address,
Relation:=3, FormulaText:="0"    ' Min Heel angle = 0 deg
    SolverAdd CellRef:=Sheets("Results").Range("$O$25").Offset(i, 0).Address,
Relation:=1, FormulaText:="35"    ' Max Heel angle = 35 deg
    SolverSolve True
    If Cells(25 + i, 19) < 0.05 Then
    Cells(25 + i, 2).Interior.ColorIndex = 0
    End If
    End If
Next i

```

References

- Drela, Mark and Harol Youngren (Nov. 2001). *XFOIL 6.9 User Primer*. Tech. rep. Aero and Astronautics Department: Massachusetts Institute of Technology. URL: https://web.mit.edu/drela/Public/web/xfoil/xfoil_doc.txt.
- Gerritsma, J., J.A. Keuning, and R. Onnick (Jan. 1993). *Sailing Yacht Performance in Calm Water and in Waves*. Tech. rep. 925-P. Ship Hydromechanics Laboratory: Delft University of Technology. URL: <http://resolver.tudelft.nl/uuid:62c1be91-8b8d-4040-90c3-c50226d48e49>.
- (November 1992). “Sailing Yacht Performance in Calm Water and in Waves”. In: *12th International Symposium on Yacht Design and Construction*. DOI: <http://resolver.tudelft.nl/uuid:62c1be91-8b8d-4040-90c3-c50226d48e49>.
- Gerritsma, J., R. Onnick, and A. Versluis (Dec. 1981). *Geometry, Resistance, and Stability of the Delft Systematic Yacht Series*. Tech. rep. 520-P. Ship Hydromechanics Laboratory: Delft University of Technology. URL: <http://resolver.tudelft.nl/uuid:b1ea34c0-a2ad-40ca-a532-c3ec094c7205>.
- Gournay, Lazare (2022). *Investigation of the Benefits of Modern Foils on an IMOCA 60 Sailing Boat*. Thesis (Master). ECN.
- Hoerner, Sighard F. (1965). *Fluid Dynamic Drag*. Hoerner Fluid Dynamics.
- ITTC (1978). *1978 ITTC Performance Prediction Method*. Tech. rep. International Tow Tank Conference. URL: <chrome-extension://efaidnbmnnnibpcajpcglclefindmkaj/https://www.ittc.info/media/8017/75-02-03-014.pdf>.
- Keuning, J.A. and U.B. Sonnenberg (Jan. 1999). *Approximation of the Calm Water Resistance of a Sailing Yacht Based on the Delft Systematic Yacht Hull Series*. Tech. rep. 1177-P. Ship Hydromechanics Laboratory: Delft University of Technology. URL: <http://resolver.tudelft.nl/uuid:5a0d1042-3b14-40ae-a0dc-cce10b1f6960>.
- ORC (2022). *ORC VPP Documentation 2022*. Offshore Racing Congress.
- (2023). *Intenational Measurement Sysetem*. Offshore Racing Congress.